Quasi-Geostrophic Response of an Infinite β-Plane Ocean to Stochastic Forcing by the Atmosphere

CLAUDE FRANKIGNOUL

Department of Meteorology, Massachusetts Institute of Technology, Cambridge 02139

PETER MÜLLER

Institut für Geophysik, Universität Hamburg, and Max-Planck-Institut für Meteorologie, Hamburg, FRG

(Manuscript received 17 April 1978, in final form 14 July 1978)

ABSTRACT

The quasi-geostrophic response of the ocean to stochastic forcing by wind stress and atmospheric pressure is investigated using a linear, continuously stratified, β-plane oceanic model with a flat bottom. We consider a spectral representation of the forcing and response fields, and we estimate the oceanic response using a vertical normal mode expansion. Model spectra of the wind stress, wind stress curl and surface pressure fields are constructed. In the wavenumber-frequency range of quasi-geostrophic eddies, the observations suggest that because of their short correlation time scale, the forcing fields are, to a reasonable approximation, white in frequency space and symmetric in wavenumber space. Forcing by the wind stress has the dominant role. The oceanic response can be off-resonant or resonant. In the off-resonant case, we predict oceanic wavenumber-frequency response spectra. In case of resonance we estimate total energy transfer rates by integrating the oceanic response over depth and wavenumber (in the range $2\pi/4000$ km^{-1}–$2\pi/50$ km^{-1}) and we distinguish between the barotropic and the total baroclinic response, the latter being obtained by summing the contribution of all baroclinic modes.

The barotropic response is resonant at practically all eddy frequencies, and the baroclinic response is resonant at frequencies smaller than the maximum frequency of the first baroclinic Rossby wave. In midlatitudes, we find comparable energy input rates into barotropic and baroclinic modes, of the order of 3×10^{-4} W m^{-2}. In high latitudes the input is comparable for barotropic Rossby waves and smaller for baroclinic ones. The total energy input rate by resonant forcing is only one order of magnitude smaller than the energy input rate from the mean atmospheric circulation into the general oceanic circulation. It is smaller, but comparable with the rate of energy conversion from the mean oceanic circulation into quasi-geostrophic eddies by barotropic and baroclinic instabilities. At medium and high frequencies, the baroclinic response is off-resonant. The model predicts red frequency spectra that are consistent with temperature observations in the central North Pacific. In particular, the seasonal variability of the observed eddy field is reproduced. A comparison with observations in the western North Atlantic also suggests that local stochastic forcing by the atmosphere is an important generating mechanism for the eddies in regions of low eddy activity.

1. Introduction

Transient fluctuations of the wind stress, buoyancy flux and pressure at the air-sea interface generate a variety of oceanic motions, including quasi-geostrophic fluctuations or "eddies" (with periods of the order of a week or more, and wavelengths of a few tens of kilometers to a few thousand kilometers), inertial oscillations, gravity waves and small-scale turbulence. The fluctuations in the atmosphere are deterministic (annual and diurnal variations) or stochastic (reflecting the day-to-day variability of the weather). In this paper, we investigate the quasi-geostrophic response of an extratropical ocean to the forcing by the stochastic component of the wind stress and atmospheric pressure fields. Stochastic forcing by buoyancy flux requires a slightly different formalism and will be investigated in Part II of this paper.

The stochastic fluctuations of the atmosphere are described by their moments or equivalently by their wavenumber-frequency spectra. Only a few frequency spectra of weathership or island station data exist for oceanic conditions, and very little information is available for the wavenumber structure of the atmospheric forcing fields above the ocean. Routine meteorological observations at sea level are available from the National Meteorological Center (NMC). They can be used to estimate the needed statistical information on the forcing fields, or conveniently taken as direct input for numerical experiments. However, the number of observing stations above the ocean is small, and the data are strongly smoothed by the NMC objective analysis

0022-3670/79/010104-24$10.00
© 1979 American Meteorological Society

scheme (Julian and Cline, 1974). Therefore, these data are most suitable to investigate the oceanic response at very large scales, and seem inappropriate to wavelengths of the order of 500 km, that characterize energetic "mesoscale" eddies observed during the POLYGON, MODE and POLYMODE experiment (e.g., Richman *et al.*, 1977). In this study, we have chosen to investigate the oceanic response analytically, using an idealized ocean-model with a flat bottom (a linear β-plane ocean of infinite horizontal extent) and a hypothetical wavenumber-frequency spectrum of the atmospheric forcing. Considerable attention has been given to reviewing the observed spectral properties of the atmospheric fields, in order to construct a model spectrum of the forcing that is not too inconsistent with the available data.

Our attempt to compute the integrated effect of atmospheric forcing distributed over a broad range of space and time scales is a novel aspect of this paper. Most previous studies consider the response of the ocean to a simple wind stress pattern, generally a large scale Fourier component with periodic or steplike time dependence. A classical reference is Veronis and Stommel (1956), who investigated the off-resonant response of an infinite, inviscid two-layer ocean to a meridionally uniform, meridional wind stress, and showed that it has increasing baroclinic character at decreasing forcing frequencies. Phillips (1966) considered the resonant and off-resonant response of a square two-layer ocean to a fluctuating, zonally uniform, zonal wind stress in the presence of bottom friction, and found that the dominant frequencies and wavenumbers of the barotropic response were consistent with the *Aries* observations near Bermuda, but that the theory underestimated largely the amplitudes. However, Leetmaa (1978) recently used the observed seasonal wind stress and suggested that the barotropic response predicted from Phillips's model was of comparable magnitude to current fluctuations observed further away from the Gulf Stream. Note that the presence of lateral boundaries causes an accumulation of energy at the western boundary of the ocean, since, as discussed, for example, by Gates (1968), the group velocity of the incoming Rossby waves is much larger than the one of the reflected waves.

In the late sixties and early seventies, less interest was shown for the effects of fluctuating winds on low-frequency oceanic motions, although much attention was given to the effects of stationary or moving storms. Veronis and Stommel (1956) had found that storms have very little effects at large depth; hence later quantitative estimates concentrated on the large and rapid response of the upper layers, using the f-plane approximation (e.g. Elsberry *et al.*, 1976). Also, the mean circulation induced by nonlinearities of the barotropic response to large-scale fluctuating winds was investigated, for example, by Veronis (1970).

Meanwhile, various kinds of evidence were accumulating to support the existence of quasi-geostrophic eddies in all regions of the ocean. These unsteady currents were first suggested by the results of the *Aries* expedition in 1959–60, and have been extensively surveyed during the POLYGON, MODE and POLYMODE experiments. The statistical properties of the eddies (energy level, dominant scales, degree of baroclinicity) may vary strongly with the geographical position (e.g., Bernstein and White, 1977; Schmitz, 1978) and different forms of mesoscale variability have been identified, such as meandering of intense currents, rings, extension rings and mid-ocean eddies. Considerable progress in understanding their dynamics has been made (cf. Rhines, 1977; MODE group, 1978). However, the dominant generating mechanisms in regions far from intense currents have not been identified. Possible candidates are topographic influences, baroclinic instability, radiation from meandering currents or rings and direct wind forcing.

The hypothesis of direct wind forcing of midlatitude eddies has generally been dismissed on the basis of the mismatch of the dominant space-time scales of atmospheric and oceanic disturbances (the atmospheric disturbances having longer wavelengths and shorter periods). However, Frankignoul and Hasselmann (1977) recently suggested that the integral effect of random, short-time scale fluctuations of the surface wind stress might generate a large low-frequency variability in the seasonal thermocline, and possibly below. At the same time, Philander (1978) proposed that large storms force a response down to the ocean floor, which interacts with the topography and results in smaller scale disturbances that could partially explain the mid-ocean eddies. Renewed interest in atmospheric forcing studies is also manifested by Magaard (1977), who suggested that direct forcing by fluctuations in wind stress and buoyancy flux may be strong enough to generate the long baroclinic Rossby waves observed in the Pacific. As discussed in detail by Philander (1978), direct forcing of barotropic and baroclinic waves becomes more efficient as one approaches the equator. However, this will not be considered here since the ocean model used in this study is not applicable to equatorial regions.

This paper is organized as follows. In Section 2, an integral form of the potential vorticity equation for quasi-geostrophic flows is derived, using projection operators (Hasselmann, 1970). This formalism allows easy inclusion and comparison of different forcing, interaction and dissipation processes. The reader who is not interested in the formal aspects of the derivation is invited to go directly to Eq (2.37), noting simply that we have replaced the usual dif-

ferential form of the potential vorticity equation by an equivalent integral form. In Section 3, the potential vorticity equation in the presence of atmospheric forcing is solved using a vertical normal mode expansion. The oceanic response is described in Section 4, and the sensitivity of the response to the model stratification is discussed. Information on the meteorological forcing fields is summarized in Section 5, and a tentative model frequency-wavenumber spectrum of the wind stress curl and surface pressure is constructed in Section 6. The oceanic response is estimated in Section 7. The barotropic response is insensitive to the model stratification, and is resonant at low and medium frequencies and off-resonant at high frequencies. The baroclinic response is resonant at low frequencies and off-resonant at medium and high frequencies. Quantitative estimates of the transfer rates and the response spectra are given. In Section 8, the model predictions are compared with field observations and the results of numerical simulation experiments. The limitations of the model and some implications of the results are discussed in Section 9.

2. The governing equations

a. Equations of motion

The quasi-geostrophic response of a stratified ocean to time-dependent forcing by the atmosphere is conveniently described by the potential vorticity equation. Here we use projection operators to derive this equation for a horizontally homogeneous extratropical ocean in the β-plane approximation. The formalism is particularly handy to investigate different forcing mechanisms and could readily be used to include interaction and dissipation processes. Since low-frequency oceanic motions are linear to lowest order (i.e., in hydrostatic and geostrophic balance), we write the equations of motion under the form

$$\frac{\partial}{\partial t} u_1 - f_0 u_2 + \frac{\partial \pi}{\partial x_1} = S_1, \tag{2.1}$$

$$\frac{\partial}{\partial t} u_2 + f_0 u_1 + \frac{\partial \pi}{\partial x_2} = S_2, \tag{2.2}$$

$$-b + \frac{\partial \pi}{\partial x_3} = S_3, \tag{2.3}$$

$$\frac{\partial}{\partial t} b + N^2 u_3 = S_4, \tag{2.4}$$

$$\frac{\partial}{\partial x_\alpha} u_\alpha + \frac{\partial}{\partial x_3} u_3 = S_5, \tag{2.5}$$

with

$$\frac{\partial}{\partial t} \zeta - u_3 = S_6 \quad \text{at} \quad x_3 = 0, \tag{2.6}$$

$$\pi - g\zeta = S_7 \quad \text{at} \quad x_3 = 0, \tag{2.7}$$

$$u_3 = S_8 \quad \text{at} \quad x_3 = -h. \tag{2.8}$$

Here, $\mathbf{x} = (x_1, x_2, x_3)$ are the coordinates (1 eastward, 2 northward, 3 upward), $\mathbf{u}$ the velocity, π the deviation of kinematic pressure (pressure per unit specific mass) from equilibrium, b the buoyancy, ζ the surface elevation, f_0 a constant value of the Coriolis parameter, $N(x_3)$ the Brunt-Väisälä or buoyancy frequency, g the gravitational acceleration and h the depth of the ocean. The source terms $S_1, \ldots, S_8$ represent the external forcing and all the terms of the equations of motion that have not been written explicitly, including dissipations, nonlinearities and deviations from the f-plane and Boussinesq approximations. Since the latters are small compared to the terms on the left hand side, they can be expressed in terms of the lowest order solution by some appropriate perturbation expansion (e.g., with respect to the Rossby number), hence considered as given "external" fields. Note that we do not make the "rigid lid approximation", which can formally be obtained by letting g tend to infinity, with N^2 remaining finite. Throughout this paper, subscripts α and β indicate 1 or 2 and repeated subscripts indicate summation.

Eq. (2.3) and (2.5) are diagnostic equations since they contain no time derivative. Hence, at any time instant, the fields u_3 and b in (2.1)–(2.8) are determined by the fields u_1, u_2 and π. However, it is more convenient to describe the flow field by the state vector

$$\Psi = \begin{pmatrix} \dfrac{\partial u_\alpha}{\partial x_\alpha} \\ \epsilon_{\alpha\beta} \dfrac{\partial u_\beta}{\partial x_\alpha} \\ f_0^{-1} \nabla^2 \pi \end{pmatrix}, \tag{2.9}$$

where $\epsilon_{\alpha\beta} = 1\ (-1)$ if α, β is an even (odd) permutation of (1,2) and zero otherwise. Here Ψ_1 is the horizontal divergence of the current field, Ψ_2 the vertical component of the relative vorticity and Ψ_3 proportional to the horizontal Laplacian $\nabla^2 = \partial^2/\partial x_\alpha \partial x_\alpha$ of the pressure. The other fields can be expressed in terms of Ψ by

$$u_1 = \nabla^{-2}\left(\frac{\partial \Psi_1}{\partial x_1} - \frac{\partial \Psi_2}{\partial x_2}\right), \tag{2.10}$$

$$u_2 = \nabla^{-2}\left(\frac{\partial \Psi_1}{\partial x_2} + \frac{\partial \Psi_2}{\partial x_1}\right), \tag{2.11}$$

$$u_3 = \int_{-h}^{x_3} dx_3' (S_5 - \Psi_1) + S_8, \tag{2.12}$$

$$\pi = f_0 \nabla^{-2} \Psi_3, \tag{2.13}$$

$$b = f_0\nabla^{-2}\frac{\partial\Psi_3}{\partial x_3} - S_3, \tag{2.14}$$

$$\zeta = g^{-1}(f_0\nabla^{-2}\Psi_3 - S_7) \quad \text{at} \quad x_3 = 0, \tag{2.15}$$

where the operator ∇^{-2} indicates $(\partial^2/\partial x_\alpha \partial x_\alpha)^{-1}$.

The interior vertical displacement $\xi = -N^{-2}b$ is readily obtained from (2.14). The equation of motion takes the form (cf. Hasselmann, 1970)

$$\frac{\partial\Psi}{\partial t} + f_0\mathbf{M}\Psi = \mathbf{q}, \tag{2.16}$$

where

$$\mathbf{M} = \begin{pmatrix} 0 & -1 & 1 \\ 1 & 0 & 0 \\ \nabla^2 L & 0 & 0 \end{pmatrix}, \tag{2.17}$$

$$\mathbf{q} = \begin{Bmatrix} \dfrac{\partial}{\partial x_\alpha} S_\alpha \\ \epsilon_{\alpha\beta}\dfrac{\partial}{\partial x_\alpha} S_\beta \\ f_0^{-1}\nabla^2\left[f_0^2 L S_5 - \displaystyle\int_{x_3}^{0} dx_3'\left(\frac{\partial}{\partial t}S_3 + S_4 - N^2 S_8\right) + g(S_8 + S_6) + \frac{\partial}{\partial t}S_7\right] \end{Bmatrix}. \tag{2.18}$$

The integral operator L comprises the effect of stratification and boundary conditions, and is defined by

$$L(A) = f_0^{-2}\left(\int_{x_3}^{0} dx_3' N^2(x_3') \int_{-h}^{x_3'} A(x_3'')dx_3'' + g\int_{-h}^{0} A(x_3')dx_3'\right), \tag{2.19}$$

where $A(x_3)$ is an arbitrary function.

b. Normal branch decomposition

The homogeneous equation

$$\frac{\partial\Psi}{\partial t} + f_0\mathbf{M}\Psi = 0 \tag{2.20}$$

has three eigensolutions or normal branches,

$$\Psi = \boldsymbol{\beta}^s \exp(-i\Omega^s t) \quad (s = 0, +, -), \tag{2.21}$$

with eigenvectors

$$\boldsymbol{\beta}^0 = \begin{pmatrix} 0 \\ 1 \\ 1 \end{pmatrix},$$

$$\boldsymbol{\beta}^s = \begin{pmatrix} is(1 - \nabla^2 L)^{1/2} \\ 1 \\ \nabla^2 L \end{pmatrix} \quad (s = +, -), \tag{2.22}$$

and eigenfrequencies

$$\Omega^s = sf_0(1 - \nabla^2 L)^{1/2} \quad (s = 0, +, -). \tag{2.23}$$

Note that $\boldsymbol{\beta}^s$ and Ω^s are operators. As discussed by Hasselmann (1970), $s = +, -$ denotes the two internal gravity wave branches, and $s = 0$ the geostrophic flow branch. In the f-plane approximation, the geostrophic flow branch has zero frequency. This degeneracy will be removed by taking into account latitudinal variations of the Coriolis parameter.

The adjoint eigenvectors or orthogonal projection operators $\tilde{\boldsymbol{\beta}}^s$ are defined by

$$\tilde{\boldsymbol{\beta}}^s \cdot \boldsymbol{\beta}^{s'} = \delta_{ss'} \quad (s, s' = 0, +, -), \tag{2.24}$$

so that

$$\tilde{\boldsymbol{\beta}}^0 = (1 - \nabla^2 L)^{-1}\begin{pmatrix} 0 \\ -\nabla^2 L \\ 1 \end{pmatrix},$$

$$\tilde{\boldsymbol{\beta}}^s = \tfrac{1}{2}(1 - \nabla^2 L)^{-1}\begin{pmatrix} -is(1 - \nabla^2 L)^{1/2} \\ 1 \\ -1 \end{pmatrix} \quad (s = +, -). \tag{2.25}$$

The eigenvectors form a complete set of vectors

$$\sum_s \beta_i^s \tilde{\beta}_j^s = \delta_{ij}.$$

The general solution $\Psi(\mathbf{x},t)$ of the inhomogeneous equation (2.16) may hence be decomposed into the three normal branches of its homogeneous form, $\boldsymbol{\psi} = \sum_s \psi^s \boldsymbol{\beta}^s$ with $\psi^s = \tilde{\boldsymbol{\beta}}^s \cdot \boldsymbol{\psi}$. The equation for the normal branch amplitude ψ^s is obtained by multiplying (2.16) from the left with $\tilde{\boldsymbol{\beta}}^s$ and takes the form

$$\frac{\partial\Psi^s}{\partial t} + i\Omega^s\Psi^s = q^s, \tag{2.26}$$

where $q^s = \tilde{\boldsymbol{\beta}}^s \cdot \mathbf{q}$ represents the projection of the source function onto the normal branch s.

c. Potential vorticity equation

In the following, we investigate the *quasi-geostrophic* response of the ocean to atmospheric

forcing. Hence, we only consider the geostrophic flow branch $s = 0$. Since the latter is characterized by a horizontally nondivergent current field ($\Psi_1^0 = 0$, where $\mathbf{\Psi}^0 = \Psi^0\boldsymbol{\beta}^0$) we introduce a streamfunction ϕ^0, defined by

$$\phi^0 = \nabla^{-2}\Psi^0 = f_0^{-1}\pi, \tag{2.27}$$

where $\psi^0 = \psi_2^0 = \psi_3^0$. Multiplying (2.26) by $(1 - \nabla^2 L)\nabla^{-2}$ and introducing the streamfunction, we obtain

$$\frac{\partial}{\partial t}(1 - \nabla^2 L)\phi^0 = Q^0, \tag{2.28}$$

where

$$Q^0 = -Lq_2 + \nabla^{-2}q_3. \tag{2.29}$$

This is an integral form of the potential vorticity equation. The usual differential form is obtained by multiplying (2.28) with L^{-1}, yielding

$$\frac{\partial}{\partial t}\left(\nabla^2 + \frac{\partial}{\partial x_3} f_0^2 N^{-2} \frac{\partial}{\partial x_3}\right)\phi^0 = q_2 + \frac{\partial}{\partial x_3} f_0^2 N^{-2} \frac{\partial}{\partial x_3}\nabla^{-2}q_3, \tag{2.30}$$

with the boundary conditions

$$\frac{\partial}{\partial t}\left(N^2 + g\frac{\partial}{\partial x_3}\right)\phi^0 = \left(N^2 + g\frac{\partial}{\partial x_3}\right)\nabla^{-2}q_3 \quad \text{at} \quad x_3 = 0, \tag{2.31}$$

$$\frac{\partial}{\partial t}\frac{\partial}{\partial x_3}\phi^0 = \frac{\partial}{\partial x_3}\nabla^{-2}q_3 \quad \text{at} \quad x_3 = -h. \tag{2.32}$$

Eq. (2.28) or (2.30) represents the potential vorticity equation in its most general form. The particular form used in this paper is obtained by specifying the source terms $S_1, \ldots S_8$ and hence the source function Q^0.

d. Source terms

We consider the oceanic response to atmospheric forcing in a β plane. The atmosphere excites oceanic motions by pressure forcing and exchange of momentum and buoyancy at the air-sea interface. Let $Q^0 = Q_\beta^0 + Q_p^0 + Q_\tau^0$ denote the source function due to β effect, atmospheric pressure and wind stress. Forcing by the buoyancy flux is not considered here.

The β effect is included by

$$S_\alpha = \epsilon_{\alpha\beta}\beta x_2 u_\beta^0 \tag{2.33}$$

which yields $Q_\beta^0 = \beta L\partial\,\phi^0/\partial x_1$.

The pressure forcing is represented in (2.7) by

$$S_7 = \rho_0^{-1}p, \tag{2.34}$$

where p is the atmospheric pressure fluctuation and ρ_0 the water density, yielding $Q_p^0 = \rho_0^{-1}f_0^{-1}\,\partial p/\partial t$. The momentum flux across the air-sea interface does not enter the potential vorticity equation directly. We make the usual assumption that this flux gives rise to body forces distributed within a thin surface layer. The momentum flux may therefore be accounted for by specifying

$$S_\alpha = \rho_0^{-1}\tau_\alpha\delta(x_3), \tag{2.35}$$

where $\tau = (\tau_1,\tau_2)$ is the surface wind stress. Using (2.19) one finds

$$Q_\tau^0 = -\rho_0^{-1}gf_0^{-2}\epsilon_{\alpha\beta}\frac{\partial\tau_\beta}{\partial x_\alpha}.$$

This source term can also be derived by applying Ekman layer theory which yields

$$S_6 = -w_E = -\rho_0^{-1}f_0^{-1}\epsilon_{\alpha\beta}\frac{\partial\tau_\beta}{\partial x_\alpha}, \tag{2.36}$$

where w_E is the Ekman suction velocity.

In summary, the integral form of the potential vorticity equation considered here is (dropping the subscript 0)

$$\frac{\partial}{\partial t}(1 - \nabla^2 L)\Phi - \beta L\frac{\partial\Phi}{\partial x_1} = Q, \tag{2.37}$$

where

$$Q(x_1,x_2,t) = \rho_0^{-1}f_0^{-1}\frac{\partial p}{\partial t} - \rho_0^{-1}f_0^{-2}g\epsilon_{\alpha\beta}\frac{\partial\tau_\beta}{\partial x_\alpha}. \tag{2.38}$$

Since u, b and π are homogenous functions of ϕ [cf. (2.10) to (2.14) with S_3, S_5, $S_8 = 0$], the atmospheric forcing function Q determines the streamfunction ϕ and hence the *interior* response of the ocean. To determine the surface elevation, the isostatic (inverse barometer) response of the sea surface should be added [cf. Eq. (2.15)].

Equation (2.37) has the same form than the equations describing the stochastic climate models of Hasselmann (1976), with Q representing the short time scale weather forcing, except for the term containing β. As discussed below, this term causes resonance of the climate system (here the ocean interior). The somewhat complex algebra of the present study reflects this additional feature.

3. Solution of the potential vorticity equation

a. Constant buoyancy frequency

Several features of the oceanic response to atmospheric forcing can be discussed by first considering a horizontally homogeneous ocean with constant buoyancy frequency $N(x_3) = N_0$, which is the simplest and analytically most convenient form of continuous stratification. Let $\phi(\mathbf{k},x_3,\omega)$ be the Fourier transform of the streamfunction, defined by

$$\phi(\mathbf{x},t) = \int d\mathbf{k}\,d\omega\,\phi(\mathbf{k},x_3,\omega) \times \exp[i(k_\alpha x_\alpha - \omega t)], \tag{3.1}$$

where $\mathbf{k} = (k_1,k_2)$. Since $\phi(\mathbf{k},x_3,\omega) = \phi^*(-\mathbf{k},x_3,-\omega)$, we consider only non-negative frequencies, $\omega \geq 0$. Let $Q(\mathbf{k},\omega)$ similarly denote the Fourier transform of the atmospheric forcing function $Q(\mathbf{x},t)$. Then, one finds from the potential vorticity equation (2.37)

$$\phi(\mathbf{k},x_3,\omega) = \frac{iQ(\mathbf{k},\omega)\cosh q(x_3 + h)}{\omega(\cosh qh + qh\epsilon^{-1}\sinh qh)}, \quad (3.2)$$

where

$$q^2 = N_0^2 f_0^{-2}(k^2 + \beta k_1\omega^{-1}). \quad (3.3)$$

Here $\epsilon = N_0^2 hg^{-1} \ll 1$ denotes the ratio of the ocean depth to the scale depth of the density and $k^2 = k_\alpha k_\alpha$. The depth-dependence of ϕ is determined by the value of qh. A given value of qh corresponds to a circle of center $(-\beta/2\omega,0)$ and radius $(\beta^2/4\omega^2 + q^2f^2N_0^{-2})^{1/2}$ in a k-plane. For qh real, or $\omega > -\beta k_1k^{-2}$, ϕ decays exponentially with depth. The oceanic response is then off-resonant or forced and, for large qh, trapped near the surface (region I in Fig. 1). For qh imaginary, or $\omega < -\beta k_1k^{-2}$, ϕ varies with depth like a cosine function (region II in Fig. 1), but becomes infinite when

$$\tanh|q|h = \frac{\epsilon}{|q|h}. \quad (3.4)$$

The resonance occurs on circles of (real) radii $[(\beta^2/4\omega_n^2) - R_n^{-2}]^{1/2}$ (see below for definitions). The resonant solutions are easily identified as planetary Rossby waves, the eigensolutions of the homogeneous potential vorticity equation. For the frequency chosen in Fig. 1, only the barotropic (indistinguishable from the circle $qh = 0$) and the first baroclinic mode (dashed circle) can be resonant.

In the rigid lid approximation, the term cosh qh in the denominator of (3.2) can be neglected. It is readily found that the rigid-lid approximation is valid everywhere in $\mathbf{k}$ plane except in a small region limited by two concentric circles of radius r such that $\beta^2/4\omega^2 - R_0^{-2} \ll r^2 \ll \beta^2/4\omega^2 + R_0^{-2}$ (indistinguishable from the circle $qh = 0$ in Fig. 1).

b. Normal mode decomposition

To evaluate the energy transfer in case of resonance and to consider a realistically stratified ocean, it is convenient to decompose the general solution of the potential vorticity equation into its normal modes. The homogeneous form of (2.37) has separable eigensolutions (Rossby waves)

$$\phi(\mathbf{x},t) = \Phi_n(x_3) \times \exp\{i[k_\alpha x_\alpha - \omega_n(\mathbf{k})t]\} \quad n = 0, 1, 2, \ldots, \quad (3.5)$$

where the vertical eigenfunctions Φ_n satisfy

$$L\Phi_n = \lambda_n\Phi_n \quad (3.6)$$

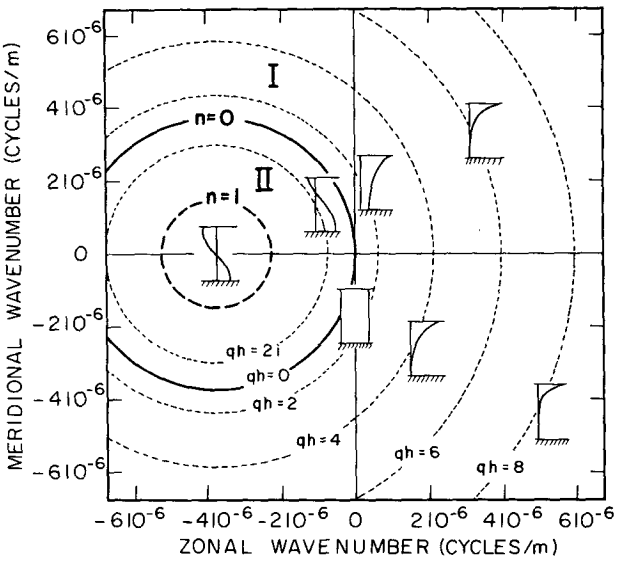

FIG. 1. Sketch of the vertical structure of the oceanic streamfunction $\phi(\mathbf{k},x_3,\omega)$ and dispersion relation (thick line) for $\omega = 2\pi/170$ day^{-1}, $N = N_0$ (see Table 1). Region I corresponds to q real, region II to q imaginary.

or equivalently[1]

$$\frac{\partial}{\partial x_3} f_0^2 N^{-2} \frac{\partial}{\partial x_3}\Phi_n = -\lambda_n^{-1}\Phi_n, \quad (3.7)$$

with

$$\left(N^2 + g\frac{\partial}{\partial x_3}\right)\Phi_n = 0 \quad \text{at} \quad x_3 = 0, \quad (3.8)$$

$$\frac{\partial}{\partial x_3}\Phi_n = 0 \quad \text{at} \quad x_3 = -h. \quad (3.9)$$

Here λ_n are the eigenvalues (constant of separation). The eigenfrequencies are given by

$$\omega_n(\mathbf{k}) = -\frac{\beta k_1}{k^2 + R_n^{-2}}, \quad (3.10)$$

where $R_n = \lambda_n^{1/2}$ denotes the Rossby radius of deformation. Values of R_n are listed for various stratifications in Table 1. Eq. (3.6) corresponds to a Sturm Liouville problem, hence the vertical eigenfunctions are complete and can be orthonormalized, i.e.,

$$\left.\begin{aligned} \int_{-h}^{0} dx_3\Phi_n\Phi_m &= \delta_{nm} \\ \sum_n \Phi_n(x_3)\Phi_n(x_3') &= \delta(x_3 - x_3') \end{aligned}\right\}. \quad (3.11)$$

Any forcing function Q (provided it can be ascribed to a body force) can be expanded with re-

[1] Derivations of Eqs. (3.7)–(3.9) can be found elsewhere, e.g., in Magaard (1977) and Flierl (1978), who make the rigid lid approximation. See also Philander (1978).

TABLE 1. Absolute value of $h^{1/2}\phi_n(0)$ and R_n for different stratifications and $h = 5000$ m, $f_0 = 7 \times 10^{-5}$ s^{-1}. The MODE values are taken from Richman *et al.* (1977) at low mode numbers and calculated in the WKB approximation (cf. Munk and Phillips, 1968) at high mode numbers. In the case of a two-layer ocean, h_1 and h_2 denote the thickness of the upper and lower layer, respectively, $\Delta\rho$ the density difference between the two layers. The value of N_0, $\tilde{\epsilon}$ and h_1 are chosen to match MODE values, as described in the text.

Stratification		$\lvert h^{1/2}\phi_n(0)\rvert$	R_n (km)
Mode profile			
$N(0) \approx 8 \times 10^{-3}$ s^{-1}	$n = 0$	1	$(gh)^{1/2}/f_0 \approx 3200$
	$n = 1$	2.9	46.7
$\bar{N} = h^{-1}\int_{-h}^{0} dx_3 N(x_3) \approx 2 \times 10^{-3}$ s^{-1}	$n = 2$	2.8	19.9
	$n = 3$	4.5	14.8
$\tilde{\epsilon} = g^{-1}h\bar{N}^2 \approx 2 \times 10^{-3}$	$n \gg 1$	$\sim(2N(0)/\bar{N})^{1/2}$	$(gh\tilde{\epsilon})^{1/2}/(f_0 n\pi)$
Constant buoyancy frequency			
$N_0 = 2 \times 10^{-3}$ s^{-1}	$n = 0$	1	$(gh)^{1/2}/f_0 \approx 3200$
$\epsilon = g^{-1}hN_0^2 = 2 \times 10^{-3}$	$n = 1$	$2^{1/2}$	46.7
	$n = 2$	$2^{1/2}$	23.4
	$n = 3$	$2^{1/2}$	15.6
	$n > 1$	$2^{1/2}$	$(gh\epsilon)^{1/2}/(f_0 n\pi)$
Two layers			
$N^2 = \tilde{\epsilon}g\delta(x_3 + h_1)$	$n = 0$	1	$(gh)^{1/2}/f_0 \approx 3200$
$\tilde{\epsilon} = \Delta\rho/\rho_0 \approx 2 \times 10^{-3}$	$n = 1$	2.9	$(gh\tilde{\epsilon}h_1h_2)^{1/2}/(f_0h_0) = 46.7$
$h_2 \approx 8.4h_1$			
Homogeneous			
$N^2 = 0$	$n = 0$	1	$(gh)^{1/2}/f_0 \approx 3200$

spect to the eigenfunctions. Hence, the solutions of the inhomogeneous potential vorticity equation (2.37) may be written

$$\phi(\mathbf{x},t) = \sum_{n=0}^{\infty} \int d\mathbf{k} a_n(\mathbf{k},t)\Phi_n(x_3) \exp(ik_\alpha x_\alpha). \quad (3.12)$$

The normal mode amplitudes a_n satisfy

$$\frac{\partial}{\partial t}(1 + k^2R_n^2)a_n - i\beta R_n^2 k_1 a_n = Q_n, \quad (3.13)$$

where

$$Q_n(\mathbf{k},t) = \frac{1}{(2\pi)^2}\int dx_1 dx_2 \exp(-ik_\alpha x_\alpha) \times \int_{-h}^{0} dx_3 \Phi_n(x_3) Q(\mathbf{x},t) \quad (3.14)$$

represents the projection of the forcing function Q into the nth eigenmode. Since Q does not depend on x_3, (3.14) may be written

$$Q_n(\mathbf{k},t) = P_n Q(\mathbf{k},t), \quad (3.15)$$

where

$$P_n = \int_{-h}^{0} dx_3 \Phi_n(x_3) = g^{-1}f_0^2 R_n^2 \Phi_n(0) \quad (3.16)$$

by use of (3.7)–(3.9). The values of $\Phi_n(0)$ are also listed in Table 1.

Eq. (3.13) can be solved by Fourier transformation in time which yields

$$a_n(\mathbf{k},\omega) = \frac{i}{\omega - \omega_n(\mathbf{k})} \frac{P_n}{1 + k^2R_n^2} Q(\mathbf{k},\omega). \quad (3.17)$$

The normal mode amplitudes a_n become infinite when frequency and wavenumber satisfy the dispersion relation (3.10). They are proportional to the atmospheric forcing function $Q(\mathbf{k},\omega)$. The factor of proportionality is determined by R_n, the Rossby radius of deformation and linearly related to $\Phi_n(0)$, the value of the normalized eigenfunctions at the surface. Table 1 demonstrates that these quantities do not depend sensitively on the stratification. In the case of constant buoyancy frequency, we have chosen the value of N_0, such that the Rossby radius of the first baroclinic mode coincides with the one of the stratification observed in the MODE region. This tuning reproduces the MODE values of R_n for $n > 1$ within 20%, and underestimates the MODE values of $\Phi_n(0)$ for the baroclinic modes $n \geq 1$ by about a factor of 2. In the following, we shall calculate the oceanic response to atmospheric forcing for an ocean with constant buoyancy frequency. This will thus provide a *conservative* estimate for the baroclinic response. Table 1 furthermore shows that the MODE value for a_0 can be reproduced with a homogeneous ocean, and that the MODE values for both a_0 and a_1 can be reproduced with a two layer ocean if the parameters $\tilde{\epsilon} = \Delta\rho/\rho_0$ and h_1 are chosen appropriately. Note that the calibration of a two-layer ocean model should be different to investigate other physical processes, like nonlinearities (Flierl, 1978).

4. Statistical representation

a. Stochastic forcing

We assume for simplicity that the stochastic component $Q_s(x_1,x_2,t)$ of the atmospheric forcing function Q is a realization of a statistically stationary and homogeneous process with zero mean and power spectrum $F(\mathbf{k},\omega)$, defined by

$$\langle Q_s(\mathbf{k},\omega)Q_s^*(\mathbf{k}',\omega')\rangle = F(\mathbf{k},\omega)\delta(\mathbf{k}-\mathbf{k}')\delta(\omega-\omega'), \quad (4.1)$$

where the angle braces denote ensemble means and the asterisk complex conjugates. The power spectrum is normalized such that $\int d\mathbf{k}\, d\omega\, F(\mathbf{k},\omega) = \langle Q_s^2(\mathbf{x},t)\rangle$. Reality, stationarity, and homogeneity imply $F(\mathbf{k},\omega) = F(-\mathbf{k},-\omega)$; hence we only consider non-negative frequencies as before. Note that the definition (4.1) implies random phases, thereby excluding standing modes. The specification of $F(\mathbf{k},\omega)$ is discussed in Sections 5 and 6. The oceanic model is linear, hence there is no need to specify the higher order statistics of the forcing function.

b. Oceanic response

The oceanic response is off-resonant or resonant. For frequencies larger than the maximum frequency $\omega_m^{\max}$ of Rossby waves, no resonance can occur [cf. Eq. (3.17)] and the oceanic response may be described in terms of power spectra. In the frequency range $\omega \leqslant \omega_m^{\max}$ there always exists a wavenumber for which the oceanic response is resonant and the spectra become infinite. The singularities could be removed by introducing dissipation mechanisms (Phillips, 1966; Magaard, 1977). However, since the precise nature of dissipation is still controversial, the resonant response is most conveniently discussed by estimating growth rates or energy transfer rates. Integrated energy transfer rates obtained by summing up the contributions from all the wavenumbers within the range of quasi-geostrophic oceanic eddies will be calculated to facilitate the comparison with estimates of the input rates of other dynamical processes. Note that the inclusion of dissipation would not affect the computed energy transfer rates, but only set the energy level of the oceanic response.

c. Off-resonant response

From (3.17) we obtain the cross spectra of the normal mode amplitudes

$$\langle a_n(\mathbf{k},\omega)a_m^*(\mathbf{k}',\omega')\rangle = \frac{1}{\omega-\omega_n(\mathbf{k})}\frac{1}{\omega'-\omega_m(\mathbf{k}')}\frac{P_n}{1+k^2R_n^2} \times \frac{P_m}{1+k'^2R_m^2}F(\mathbf{k},\omega)\delta(\mathbf{k}-\mathbf{k}')\delta(\omega-\omega'). \quad (4.2)$$

Cross spectra of all oceanic variables can easily be derived from this relation, using (3.12), (2.27) and (2.10)–(2.15). For frequencies much larger than the frequencies of Rossby waves, the oceanic spectra are red and behave like ω^{-2}. This is a general feature of the response of the long time scale "climate" system to the short time scale variability of the "weather" (Hasselmann, 1976).

The maximum frequency for each normal mode is reached when $k_1 = R_n^{-1}$ and $k_2 = 0$, and is given by $\omega_n^{\max} = \beta R_n/2$. For values characteristic of the MODE region ($\beta = 2 \times 10^{-11}$ m^{-1} s^{-1}, R_n as given in Table 1) and for a wavenumber $k \geqslant 2\pi/4000$ km^{-1} one finds $\omega_0^{\max} \approx 1.2\ 10^{-5}$ s^{-1} (minimum period $T^{\min} \approx 6$ days), $\omega_1^{\max} \approx 4.7\ 10^{-7}$ s^{-1} ($T_0^{\min} \approx 156$ days), and $\omega_n^{\max} < \omega_1^{\max}$ for $n = 2, 3, \ldots$. The barotropic response is thus resonant throughout the frequency range of quasi-geostrophic eddies. On the other hand, the baroclinic response is off-resonant in a much broader frequency range, and the calculation of forced spectra is of direct use. An illustration is given in Section 8. Here we shall only emphasize the need to take into account the contributions of all baroclinic modes, hence to consider a continuously stratified ocean when investigating its baroclinic response to transient atmospheric forcing.

Using the orthogonality relations (3.11), the spectrum of the depth-integrated total energy, defined by

$$E_{\text{tot}}(x_1,x_2,t) = \tfrac{1}{2}\rho_0\int_{-h}^{0} dx_3(u_\alpha u_\alpha + N^{-2}b^2) + \tfrac{1}{2}\rho_0 g\zeta^2 \quad (4.3)$$

can be written

$$E_{\text{tot}}(\mathbf{k},\omega) = \sum_{n=0}^{\infty} E_{\text{tot}}^n(\mathbf{k},\omega), \quad (4.4)$$

where

$$E_{\text{tot}}^n(\mathbf{k},\omega) = \tfrac{1}{2}\rho_0\frac{1}{(\omega-\omega_n)^2} \times \frac{P_n^2}{R_n^2(1+k^2R_n^2)}F(\mathbf{k},\omega) \quad (4.5)$$

represents the energy spectrum of the nth mode. The depth-integrated kinetic energy spectrum of the nth mode is given by

$$E_{\text{kin}}^n(\mathbf{k},\omega) = \frac{k^2R_n^2}{1+k^2R_n^2}E_{\text{tot}}^n(\mathbf{k},\omega) \quad (4.6)$$

consistent with Gill *et al.* (1974). If we assume constant buoyancy frequency, the ratio $r_{n,m}(\mathbf{k})$ of energy in the nth and mth baroclinic mode is given by

$$r_{n,m}(\mathbf{k}) = \frac{k^2 + R_m^{-2}}{k^2 + R_n^{-2}} \quad (\omega \gg \omega_n, \omega_m). \quad (4.7)$$

For small k ($k \ll R_n^{-1}, R_m^{-1}$), most of the energy is in the lowest mode ($r_{n,m} \approx R_n^2/R_m^2$) but for large k ($k \gg R_n^{-1}, R_m^{-1}$), the energy is equally distributed among the baroclinic modes. Summing the oceanic response over the first few modes only would therefore be erroneous at high wavenumbers.

D. Resonant response

To estimate the energy transfer rates of the resonant oceanic response we solve Eq. (3.13) by

$$a_n(\mathbf{k},t) = \frac{P_n}{1 + k^2R_n^2}\int_0^t dt' e^{i\omega_n(t'-t)}Q_s(\mathbf{k},t') = \frac{P_n}{1 + k^2R_n^2}\int d\omega Q_s(\mathbf{k},\omega)\Delta(\omega - \omega_n)e^{-i\omega_n t}, \quad (4.8)$$

where

$$\Delta(\omega) = \frac{1 - e^{-i\omega t}}{i\omega}.$$

The spectra of the normal amplitudes are then given by

$$\langle a_n(\mathbf{k},t)a_n^*(\mathbf{k}',t)\rangle = \frac{P_n^2}{(1 + k^2R_n^2)^2}\int d\omega d\omega' F(\mathbf{k},\omega)\delta(\omega - \omega') \times \delta(\mathbf{k} - \mathbf{k}')\Delta(\omega - \omega_n)\Delta^*(\omega' - \omega_n) = 2\pi t \frac{P_n^2}{(1 + k^2R_n^2)^2} F(\mathbf{k}, \omega = \omega_n)\delta(\mathbf{k} - \mathbf{k}'), \quad (4.9)$$

where we have used $\lim_{t\to\infty}\Delta(\omega)\,\Delta^*(\omega) = 2\pi t\delta(\omega)$. The linear growth of the power spectrum is a general feature of the resonant response of an undamped linear system to stochastic external forcing (cf. Hasselmann, 1967). From (4.9) we obtain the growth rate of the depth-integrated total energy spectrum in case of resonance, i.e.,

$$\frac{\partial}{\partial t}E^n_{\text{tot}}(\mathbf{k},t) = \rho_0\pi\frac{P_n^2}{R_n^2(1 + k^2R_n^2)}F(\mathbf{k}, \omega = \omega_n). \quad (4.10)$$

The transfer function between the oceanic energy spectra and the atmospheric forcing spectrum depends only on R_n and $\Phi_n(0)$, as was the case for the normal mode amplitudes. Hence, the depth integrated spectra are also fairly insensitive to the choice of the model stratification. The latter mainly determines the distribution of energy with depth.

To estimate the total energy transfer rates into quasi-geostrophic eddies, we make a spectral integration in wavenumber space between $k_m = 2\pi/4000$ km^{-1} and $k_m = 2\pi/50$ km^{-1}. The lower integration limit is sufficiently large for the β plane approximation to remain valid. The upper integration limit corresponds to the grid size of an eddy resolving general circulation model (EGCM) of the ocean and is large enough for the hydrostatic approximation to remain valid. In polar coordinates the barotropic response is given by

$$\frac{\partial}{\partial t}E^0_{\text{tot}}(t) = 2\pi\int_0^{2\pi} d\theta \times \int_{k_m}^{k_M} dk k T^0(k)F(\mathbf{k}, \omega = \omega_0), \quad (4.11)$$

with

$$T^0(k) = \tfrac{1}{2}\rho_0 g^{-2}h^{-1}f_0^4(k^2 + R_0^{-2})^{-1}. \quad (4.12)$$

The observations suggest that the atmospheric forcing spectrum $F(\mathbf{k},\omega)$ is approximately white in the frequency range of quasi-geostrophic motions, hence $F(\mathbf{k},\omega) \approx F(\mathbf{k},0)$ (cf. Section 5). In this case, (4.11) may be written

$$\frac{\partial}{\partial t}E^0_{\text{tot}}(t) = 2\pi\int_{\pi/2}^{3\pi/2} d\theta \int_{k_m}^{k_M} dk k T^0(k)F(\mathbf{k},0), \quad (4.13)$$

where we have limited the integration to westward propagating disturbances in order to satisfy the resonance condition for Rossby waves.

As demonstrated above, the baroclinic response will be underestimated by only considering the first few modes. We thus define the total energy transfer rate into all baroclinic modes by

$$\frac{\partial}{\partial t}E^{bc}_{\text{tot}}(\mathbf{k},t) = \sum_{n=1}^{\infty}\frac{\partial}{\partial t}E^n_{\text{tot}}(\mathbf{k},t). \quad (4.14)$$

For an ocean with constant buoyancy frequency, the integrated energy transfer takes the simple form

$$\frac{\partial}{\partial t}E^{bc}_{\text{tot}}(t) = 2\pi\int_{\pi/2}^{3\pi/2} d\theta \int_{k_m}^{k_M} dk k T^{bc}(k)F(\mathbf{k},0), \quad (4.15)$$

with

$$T^{bc}(k) = \tfrac{1}{2}\rho_0 g^{-2}h^{-1}f_0^4 k^{-2}(y\coth y - 1). \quad (4.16)$$

and $y = \pi R_1 k$. Fig. 2 shows that the barotropic response dominates at low wavenumbers ($k \ll R_1^{-1}$) and the baroclinic response dominates at high wavenumbers ($k > R_1^{-1}$).

5. Meteorological input

In midlatitudes the dominant time scale of the atmospheric fields is a few days and most of the air-sea exchanges are associated with the eastward traveling frontal cyclones and anticyclones, which have wavelengths from 3000 to 6000 km. However, the forcing of the ocean is not confined to the very

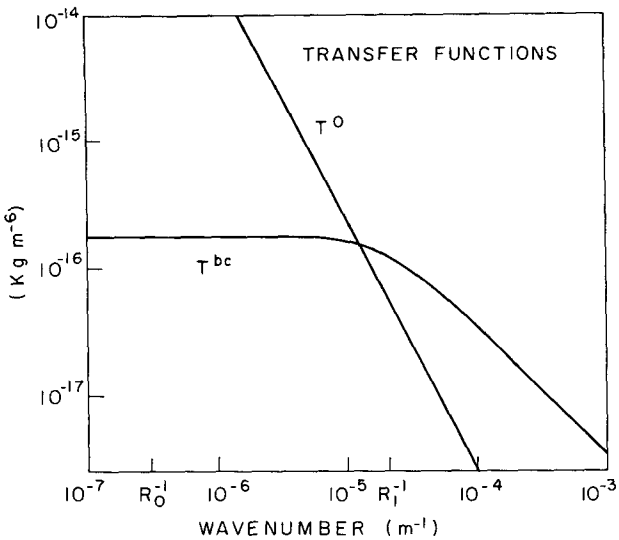

FIG. 2. Transfer functions $T^0(k)$ and $T^{bc}(k)$ for $N = N_0$ (see Table 1).

energetic weather system band, and atmospheric spectra have significant energy at lower frequencies and higher wavenumbers.

Except for the annual peak[2], atmospheric spectra in mid and high latitudes are approximately white at periods >10–20 days, as illustrated in Fig. 3, which represents the frequency spectrum $F(\omega) = \int d\mathbf{k}\ F(\mathbf{k},\omega)$ of atmospheric pressure at Ocean Weathership N (after Dorman, 1974) (see also Figs. 5 and 6). The whiteness of low-frequency spectra is due to the fact that processes with a short correlation time scale normally have a frequency spectrum which is white at sufficiently low frequencies (e.g., Hasselmann, 1976). This whiteness is also found in zonal wavenumber-frequency spectra $F(k_1,\omega) = \int dk_2 F(\mathbf{k},\omega)$ of tropospheric data. For example, the frequency spectra of geopotential height and temperature in the troposphere computed by Willson (1975) for each zonal wavenumber m (the number of waves around a latitude circle) are white at frequencies below some "cutoff" frequency which generally increases with m. The corresponding periods range from one month at the lowest wavenumbers to a few days for large m (see also Pratt, 1975). Thus, even at large scales, long time scale atmospheric disturbances like blocking ridges do not seem to dominate the observed variability at low frequencies (except in some regions, perhaps), and most of the variance is due to the "low-frequency white noise extension" of the rapidly varying weather fluctuations.

If the atmospheric variability at low frequencies is mostly due to the short time scale weather fluctuations, the covariance function $Z(\mathbf{r},\tau) = \langle v_i(\mathbf{x} + \mathbf{r}, t + \tau)\, v_j(\mathbf{x},t)\rangle$ between variables v_i and v_j vanishes for time lag $\tau > \tau_x$, where τ_x is some short characteristic time (possibly dependent on $\mathbf{r}$). Then the wavenumber-frequency spectrum

$$F(\mathbf{k},\omega) = \frac{1}{(2\pi)^3}\int_{-\infty}^{\infty} d\mathbf{r}d\tau Z(\mathbf{r},\tau)\exp[-i(\mathbf{k}\cdot\mathbf{r} - \omega t)]$$

is normally white at frequencies $\omega \ll \tau_x^{-1}$, for $F(\mathbf{k},0) \neq 0$, since the exponential $e^{i\omega\tau}$ can be set equal to 1. Hence, one can write

$$\lim_{\omega\to 0} F(\mathbf{k},\omega) = F(0)S(\mathbf{k}),$$

where $F(0) = \int d\mathbf{k}\ F(\mathbf{k},\ \omega = 0)$ is the *white noise level* and $S(\mathbf{k})$ the normalized wavenumber structure, $\int d\mathbf{k}\ S(\mathbf{k}) = 1$. Spectra are positive-definite functions. From the reality condition $F(\mathbf{k},\omega) = F^*(\mathbf{k},\omega) = F(-\mathbf{k},-\omega)$, it then follows that the spectra are symmetric at low frequencies. This contrasts with the well-known asymmetry of the atmospheric fields at short periods, synoptic and planetary scales, which reflects in midlatitude the eastward propagation of cyclones and anticyclones. Symmetry can also be demonstrated from observations, since the propagation direction of atmospheric disturbances has been inferred from zonal wavenumber-frequency analysis of tropospheric data. Notice that only east-west asymmetries can be estimated and not the partition into standing and propagating disturbances (Pratt, 1976). Willson (1975)'s analysis of temperature at 500 mb (45°N) suggests that at periods >10 days, the symmetric part of the spectra dominates the asymmetric one at $m \gtrsim 7$. Similarly, Pratt and Wallace (1976) found that the ratio of propagating variance (excess of variance in one of the two directions) to total variance of the 500, 850 and 1000 mb geopotential height and

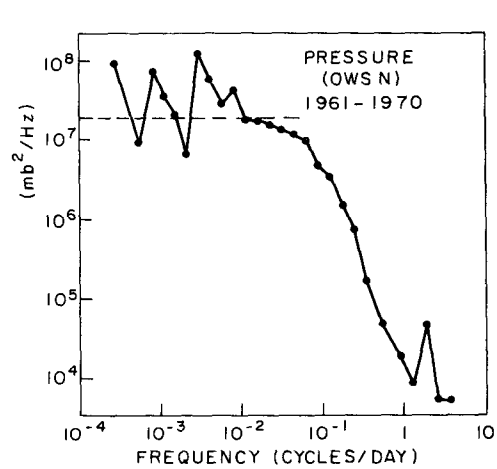

FIG. 3. Spectrum of pressure at OWS N computed from 10 years of data (after Dorman, 1974). The dashed line shows the white noise level given in Table 1.

[2] Note that artificial redness is introduced at low frequencies when the annual signal is not resolved or filtered.

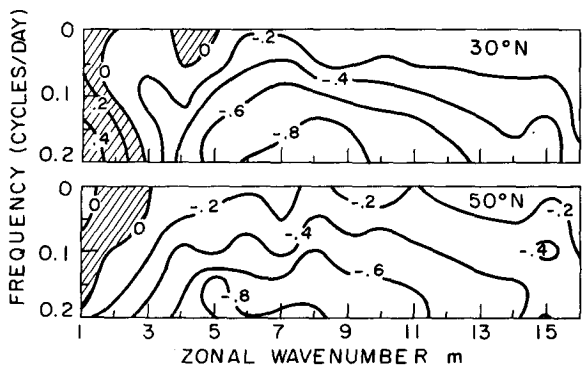

FIG. 4. Ratio of propagating to total variance for 1000 mb geopotential height at 30 and 50°N. The data are based on two 6-month winters and are unfiltered. Positive values (hatched) indicate westward propagation. The contours were drawn subjectively on the basis of data communicated by R. W. Pratt.

temperature is small in midlatitudes at periods >10 days, except around zonal wavenumbers 6–9 where disturbances propagate preferably eastward (Fig. 4). At higher values of m, there is also a weak tendency toward preferred eastward propagation, but the asymmetry seems to decay both with decreasing frequency and increasing wavenumber. At a period of 20 days and $m > 8$ ($\lambda_1 < 3200$ km), 80% of the energy is in motions symmetric in the mean (see also Blackmon, 1976). Recently Willebrand (1978) investigated the symmetry of surface pressure and geostrophic wind stress disturbances above the North Pacific and Atlantic oceans (NMC data), by means of cross-spectral analysis of times series at different locations. At periods >10 days, he also found no preferred propagation direction. Hence, atmospheric spectra are, to a reasonable approximation, white and symmetric in the wavenumber-frequency range of oceanic eddies. This symmetry has important consequences, since it implies that atmospheric disturbances can resonantly excite westward propagating oceanic Rossby waves.

To construct a model wavenumber-frequency spectrum of the atmospheric forcing function Q_s, we still need information on the white noise level of the atmospheric spectra and on their wavenumber structure $S(\mathbf{k})$. Some relevant information is reviewed below.

As one approaches the equator, the characteristic time scale of the atmospheric variables becomes more difficult to define but increases. The formulation of a model wavenumber-frequency spectrum of the atmospheric forcing thus requires a slightly different approach.

a. White noise level

Ocean weathership (OWS) and island station data provide information on the frequency spectrum of the atmospheric forcing function above the ocean and hence on the white noise level $F(0)$. Table 2 summarizes observations on wind, wind stress, wind stress curl and atmospheric pressure at latitudes higher than 15°. A few wind spectra have been

TABLE 2. Atmospheric frequency spectra in extratropical oceanic conditions. U_{x_3} ($\mathbf{U}_{x_3}$) denotes the wind speed (vector) at height x_3 in meters (given when known). $F(0)$ is an estimate of the approximately constant spectral density of the variance at low frequencies; for vector quantities, $F(0)$ is the sum of the spectral density of each component. C and C_{10} are drag coefficients. "Slightly red" indicates a spectral slope ≤0.5 and apr (apnr) that the annual peaks are (are not) resolved. Corrections for wind level are based on a neutral log wind profile.

Author	Data	Data source	Location	Duration (sampling)	$F(0)$	Comments
Baker *et al.* (1977)	U_i	Surface pressure analysis	59°S, 63°W (Drake Passage)	308 days (12 h)	4×10^7 m^2 s^{-2} Hz^{-1}	Geostrophic wind in the through-passage direction only (aprn)
Frost (1975)	U_{10}	Weathership *India*	59°N, 19°W (Atlantic)	26 years (3 h)	10^7 m^2 s^{-2} Hz^{-1}	Slightly red at period >2 years (apr)
Willebrand (1978)	$\mathbf{U}_{10}$	Weathership C	52°N, 35°W (Atlantic)	26 years (12 h)	6×10^7 m^2 s^{-2} Hz^{-1}	East wind slightly more energetic (aprn)
	τ				6×10^4 N^2 m^{-4} Hz^{-1}	East stress twice more energetic; linear drag law (apr)
	P				2×10^8 mb^2 Hz^{-1}	(apr)
Fissel *et al.* (1976); also Fissel (1975)	U_{22}	Weathership P	50°N, 145°W (Pacific)	10 years (3 h)	7×10^6 m^2 s^{-2} Hz^{-1}	Wind reduced to 10 m level (apr)
	$\mathbf{U}_{22}$				4×10^7 m^2 s^{-2} Hz^{-1}	*ibid.*
	τ				3×10^4 N^2 m^{-4} Hz^{-1}	$C_{10} = 1.5 \times 10^{-3}$ assumed here (apr)
	P				10^8 mb^2 Hz^{-1}	(apr)
Byshev and Ivanov (1969)	U	Weatherships C and D	52°N, 35°W 44°N, 41°W	3 years (6 h)	~10^7 m^2 s^{-2} Hz^{-1}	Average spectra, slightly red (apnr)

TABLE 2. (*Continued*)

Author	Data	Data source	Location	Duration (sampling)	$F(0)$	Comments
Willebrand (1978)	U_{10}	Surface pressure analysis	Longitudinal average over North Pacific at 43°N	4 years (12 h)	3×10^7 m^2 s^{-2} Hz^{-1}	Geostrophic wind reduced to the surface; east wind twice as energetic (apnr)
	τ				3×10^4 N^2 m^{-4} Hz^{-1}	East stress twice as energetic; linear drag law (apnr)
	P				$\sim 5 \times 10^7$ mb^2 Hz^{-1}	Slightly red (apnr)
	$\epsilon_{\alpha\beta}(\partial/\partial_\alpha)\tau_\beta$				2×10^{-8} N^2 m^{-6} Hz^{-1}	(apnr)
Wunsch (1972)	U	National Weather Record Center	32°N, 65°W (Bermuda)	8 years (1 h)	$\sim 3 \times 10^7$ m^2 s^{-2} Hz^{-1}	Wind measured at 11 m (3*y*), 4 m (3*y*) and 5 m (2*y*) above ground; no corrections made, about 10% underestimated (apnr)
	τ				10^4 N^2 m^{-4} Hz^{-1}	$C_{10} = 1.5 \times 10^{-3}$ assumed here; wind not converted to 10 m level, about 25% underestimated (apnr)
	P				$\sim 4 \times 10^7$ mb^2 Hz^{-1}	Slightly red (apnr)
Dorman (1974)	U_{25}	Weathership N	30°N, 140°W	10 years (3 h)	4×10^6 m^2 s^{-2} Hz^{-1}	Wind reduced to 10 m level (apr)
	U_{25}				10^7 m^2 s^{-2} Hz^{-1}	*ibid.*
	P				2×10^7 mb^2 Hz^{-1}	(apr)
Düing *et al.* (1977)	$\epsilon_{\alpha\beta}(\partial/\partial_\alpha)\tau_\beta$	Surface wind at four coastal stations	Between 25 and 30°N, 98 and 80°W (Florida and Texas)	26 months (1 day)	$\sim 4 \times 10^{-9}$ N^2 m^{-6} Hz^{-1}	$C = 1.5 \times 10^{-3}$ (apnr)
D. Luther (unpublished)	U_{10}	National Climatic Center	28°N, 177°W (Midway)	4 years (1 h)	3×10^7 m^2 s^{-2} Hz^{-1}	East wind twice as energetic (apr)
	τ				3×10^3 N^2 m^{-4} Hz^{-1}	East stress four times as energetic; linear drag law with varying roughness length (apr)
	P				2×10^7 mb^2 Hz^{-1}	(apr)
Brooks and Mooers (1977)	τ	Surface wind at a coastal station	25°N, 80°W (Miami)	4 months (3 h)	$\sim 3 \times 10^2$ N^2 m^{-4} Hz^{-1}	Summer only; $C = 2 \times 10^{-3}$ (apnr)
D. Luther (unpublished)	U_{10}	National Climatic Center	19°N, 167°W (Wake)	4 years (1 h)	$\sim 2 \times 10^7$ m^2 s^{-2} Hz^{-1}	East wind slightly red and more energetic (apr)
	τ				$\sim 7 \times 10^3$ N^2 m^{-4} Hz^{-1}	East stress slightly red and more energetic; linear drag low with varying roughness length (apr)
	P				$\sim 4 \times 10^6$ mb^2 Hz^{-1}	Slightly red (apr)

listed to better document the geographical variability of the atmospheric fields. In general, the white noise level decreases from higher to lower latitudes (see also Willebrand, 1978). Additionally, the white noise level of the wind stress (and presumably of the wind stress curl) seems to increase with the magnitude of the mean wind. This is seen by comparing spectra at Midway (small mean wind) and Wake (large mean wind). Fig. 5 shows for illustration the wind stress variance spectrum at OWS *P* (50°N, 145°W) (after Fissel, 1975). Düing *et al.* (1977) estimated the wind stress curl from observed winds at Jacksonville, Miami, Key West and Corpus Christi (Fig. 6). They used wind stress differences between stations approximately 1800 and 700 km apart in the zonal and meridional directions, respectively. However, the wind stress curl variance is concentrated in relatively small scales (Welch, 1972; Saunders, 1976). Hence, the "white noise level" of Düing *et al.* (1977) considerably underestimates the wind stress curl energy density above the ocean since only rather large scales contributed to their estimates. Furthermore, the wind stress curl is much smaller near the coast than above the open ocean (Saunders,

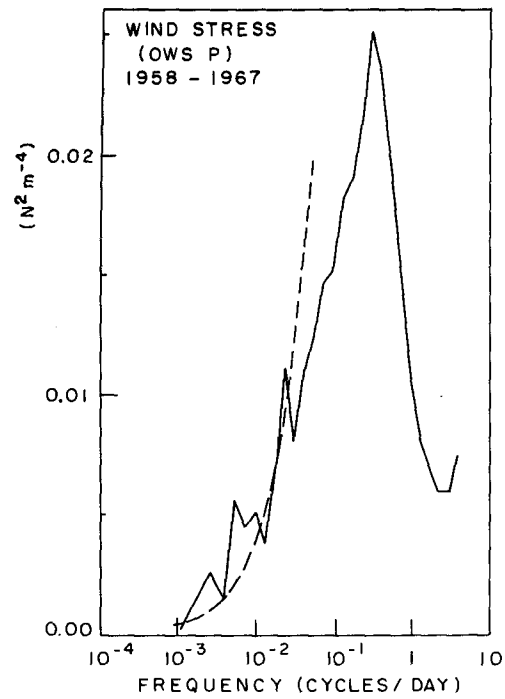

FIG. 5. Variance-conserving plot of the wind stress spectrum $F_{\tau_1\tau_1}(\omega) + F_{\tau_2\tau_2}(\omega)$ at OWS P computed from five 2-year data blocks (after Fissel, 1975). The dashed line shows the white noise level given in Table 1. We have assumed $C_{10} = 1.5 \times 10^{-3}$.

1977). Similarly, the white noise level of the wind stress curl in Willebrand (1978) (Table 2) is low because of the severe smoothing of the NMC surface pressure field data used to compute the geostrophic wind. The coherence between wind, wind stress and pressure is generally poor at low frequencies because of symmetry (Fissel, 1975; Willebrand, 1978).

Seasonal variations in the low-frequency "white noise level" of the atmospheric spectra may be important. In the Northern Hemisphere the energy level of the wind, wind stress and pressure are generally three or four times higher in fall and winter than in spring and summer (cf. Dorman, 1974; Fissel, 1975; Fissel *et al.*, 1976; and Fig. 12). On the other hand, there might be much less seasonal variation in the Southern Hemisphere (cf. Kao *et al.*, 1970).

b. Wavenumber structure

A considerable amount of wavenumber and wavenumber-frequency spectra of geopotential height, geostrophic wind and temperature is available for large-scale tropospheric motions along latitude circles. Two-dimensional wavenumber spectra have also been calculated by means of spherical harmonic expansion.

Blackmon's (1976) analysis of the 500 mb geopotential height in the Northern Hemisphere suggests that low-frequency kinetic energy is maximum at two-dimensional wavenumber 8 ($\lambda = 5000$ km). Analyzing balloon data, Desbois (1975) found that midlatitude wind kinetic energy spectra at the 200 mb level have a maximum at zonal wavenumbers $m = 5$ or $m = 6$ ($\lambda_1 \approx 5000$ km at 45°S) and decay as $k_1^{-2.9}$ for $8 \leq m \leq 35 \equiv m_{\max}$, the limit of his analysis (4000 km $\geq \lambda_1 \geq$ 800 km). The decay is consistent with the k^{-3} behavior predicted by two-dimensional and quasi-geostrophic turbulence theories (Kraichnan, 1967; Charney, 1971). These theories suggest that the observed spectral decay law extends to higher wavenumbers. Using unsmoothed NMC data, Julian and Cline (1974) found similar results ($m_{\max} = 18$). A slight decrease of the high wavenumber slope with decreasing altitude—2.9 at 200 mb, −2.8 at 500 mb and −2.7 at 850 mb (mean for summer and winter)—can be seen in their analysis. Most other published spectra have been determined by using the objectively analyzed geopotential height NMC data, and are strongly affected by a loss of variance at the higher wavenumbers (Julian and Cline, 1974). Among others, Pratt (1975) has computed frequency-wavenumber spectra of the geostrophic wind at several levels and latitudes. Low-frequency geostrophic wind spectra at 850 and 1000 mb are reproduced in Fig. 7. They also suggest that the spectral decay at high wavenumbers is less rapid near the ground. This may be due to the frequent passage of surface fronts (discontinuities). Andrews and Hoskins (1978) have predicted that fronts cause a −8/3 spectral decay, consistent with observations at latitudes higher than 35°. At lower latitudes, the spectral decay is not so steep.

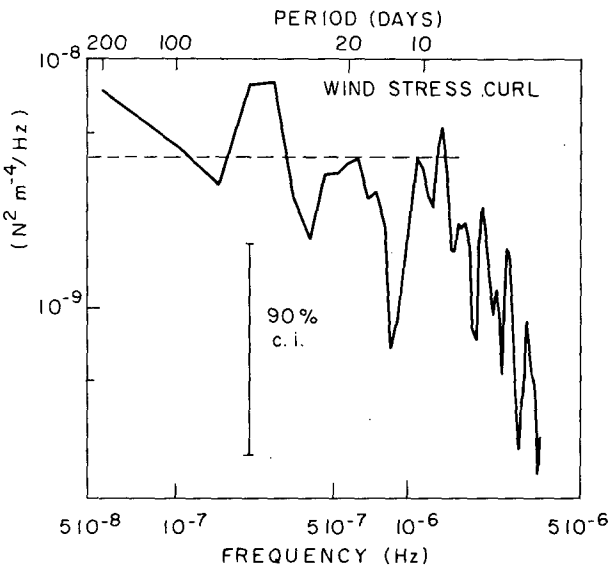

FIG. 6. Spectrum of the wind stress curl estimated from four coastal stations around the Gulf of Mexico and computed from three 200-day data blocks (after Düing *et al.*, 1977). The dashed line shows the white noise level given in Table 1.

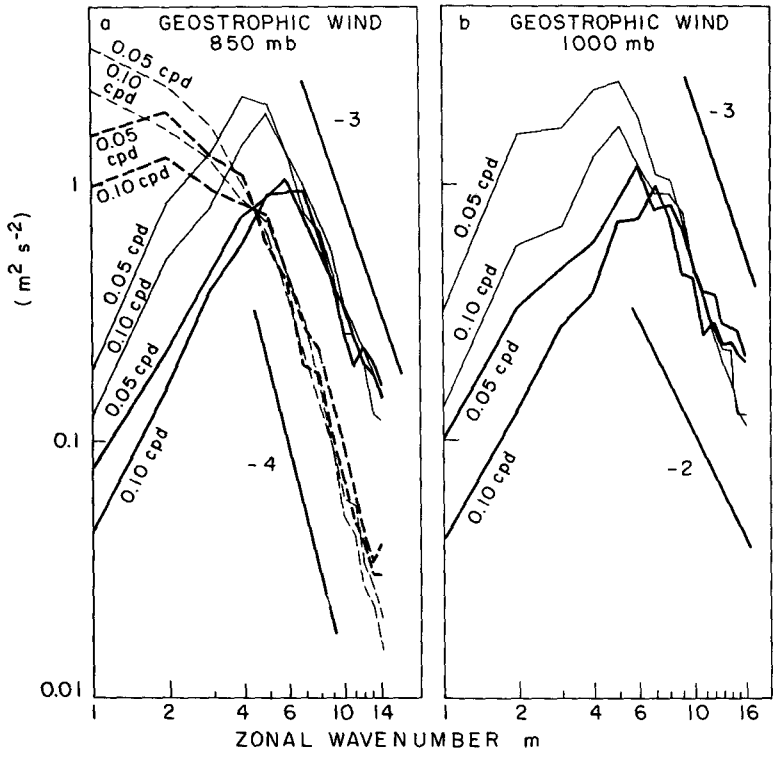

FIG. 7a. Low-frequency zonal wavenumber spectra of zonal (dashed line) and meridional (solid line) geostrophic wind at 35°N (thick line) and 50°N (thin line), and 850 mb. The spectra were computed from four 132-day winters, after high-pass filtering to remove seasonal effects.

FIG. 7b. Low-frequency zonal wavenumber spectrum of meridional geostrophic wind at 30°N (thick line) and 50°N (thin line), and 1000 mb. The spectra were computed from two 6-month winters, without filtering [constructed from Pratt (1975 and private communication)]. The straight lines indicate different spectral slopes.

This is illustrated in Fig. 8 (after Kao, private communication) which represents kinetic energy spectra computed at different latitudes from the pressure field at 850 and 1000 mb, using NMC data. Notice also the increase in energy level with increasing latitude. Kao has also computed kinetic energy spectra from the pressure field over the North Pacific only (dashed line in Fig. 8). There is little difference in spectral shape (North Pacific values at $m = 1,2$ are of course not representative). The energy density, however, is generally larger over the North Pacific than over the whole latitudinal circle, which is consistent with the higher energy density generally reported for the wind above the ocean (see Blackmon, 1976). Hence, information on the wavenumber structure of the oceanic wind field may reasonably be derived from planetary data.

Little information is available on the wavenumber structure of the wind stress and wind stress curl. Willebrand (1978) has suggested that the wavenumber spectrum of the wind stress should be slightly less steep than that of the wind. Frankignoul and Hasselmann (1977, Fig. 2) estimated wavenumber spectra of the meridional wind stress and the wind stress curl from simulated data generated by a numerical model of two-dimensional barotropic turbulence. The poor spatial resolution severely limits the representativity of the spectra (especially for the wind stress curl), but this computation suggests that the high wavenumber decay of the wind stress spectrum is similar to the one of the wind.

c. *Isotropy*

At the synoptic and planetary scales, the wind and wind stress fields are predominantly zonal. This anisotropy decreases with increasing wavenumber. Desbois (1975) has shown that the assumption of isotropy becomes partially valid in the range $2000 < \lambda_1 < 3000$ km, and is fully valid at smaller scales. Similar properties are expected from the wind stress. The overall effects of the low wavenumber anisotropy [as estimated by comparing $F(0)$ for zonal and meridional stress] is generally small, but becomes important as the trade wind region is approached (Table 2).

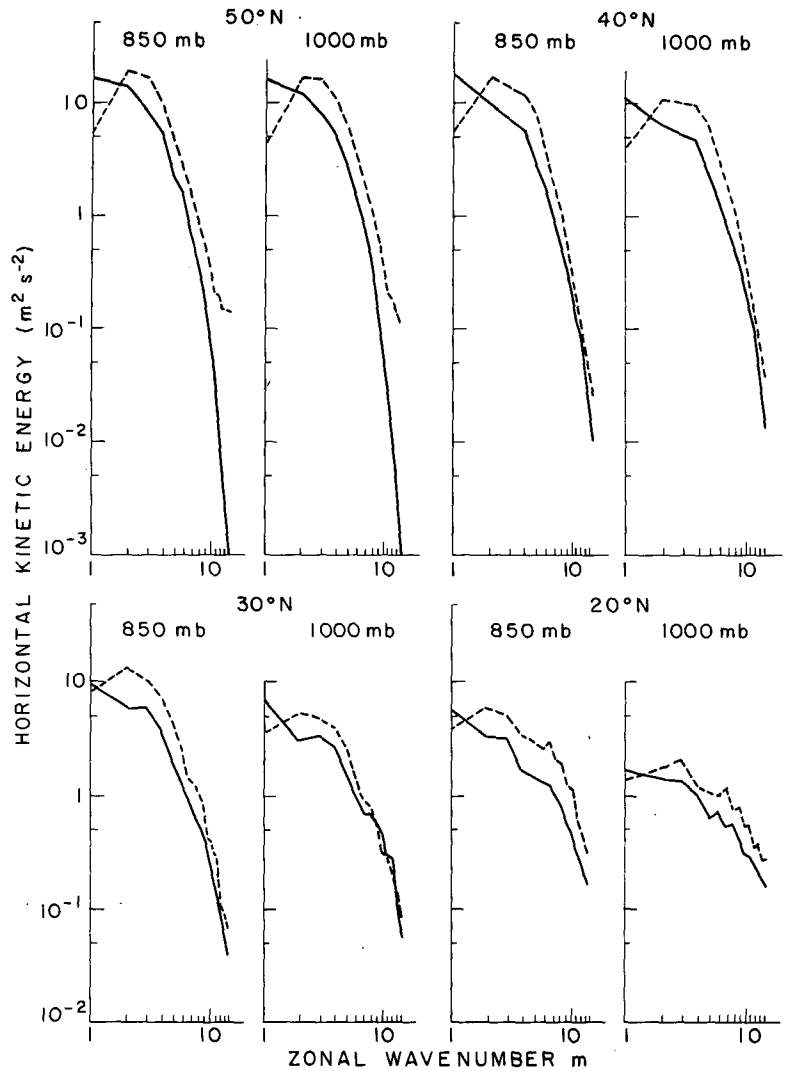

FIG. 8. Zonal wavenumber spectra of horizontal kinetic energy of the geostrophic wind at 850 and 1000 mb, at different latitudes. The spectra were computed from one 64-day winter. Solid lines: spectra over a whole latitudinal circle; dashed lines: spectra over the North Pacific only (after Kao, private communication).

6. Representation of the atmospheric spectra

In view of the sparsity of the information on the atmospheric fields above the ocean and their complexity, the construction of an analytically convenient model spectrum of the atmospheric forcing function is admittedly subjective and other representations could have been favored. Making drastic simplifications, we assume here that the atmospheric forcing function Q_s is statistically stationary and homogeneous. To represent the seasonal changes in the intensity of the atmospheric fields and their latitudinal nonhomogeneity, we postulate a parametric nonhomogeneity: we choose different spectral levels for different seasons (Section 8), and different model spectra for mid and high latitudes (say, the delimitation is ~35°).

We also assume that in the wavenumber-frequency range of quasi-geostrophic eddies, the atmospheric spectra are white in frequency domain, and symmetric, so that they take the form (5.1) with $S(\mathbf{k}) = S(-\mathbf{k})$. As discussed in Section 5, the assumption of whiteness and symmetry is justified at low frequencies or high wavenumbers, and not unreasonable in the high frequency, small wavenumber part of the eddy range.

a. Wind stress

For convenience, we assume that the wind stress field is isotropic, so that

$$S(\mathbf{k}) = (1/2\pi k)S(k), \qquad (6.1)$$

hence

$$\lim_{\omega\to 0} F(\mathbf{k},\omega) = (1/2\pi k)F(0)S(k) = (1/2\pi k)F(k,\omega). \quad (6.2)$$

As discussed in Section 5, the wind stress field is isotropic at medium and small scales, but not at the largest scales. Since the transfer functions (4.12) and (4.16) depend on wavenumber magnitude only, an anisotropic forcing will cause an anisotropic response, but the anisotropy will not affect the integrated oceanic response considered below. We thus assume isotropy for algebraic simplicity in this section.

The general form of the wind spectrum is then

$$F_{\tau_\alpha\tau_\beta}(\mathbf{k},\omega) = \frac{C}{2\pi k}\left[S_\tau(\mathbf{k})\delta_{\alpha\beta} + S'_\tau(k)\frac{k_\alpha k_\beta}{k^2}\right], \quad (6.3)$$

where C is defined such that $\int dk(F_{\tau_{11}} + F_{\tau_{22}}) = F_\tau(0)$, the white noise level of the wind stress variance $F_{\tau_1\tau_1}(\omega) + F_{\tau_2\tau_2}(\omega)$. We assume nondivergence, as suggested by surface wind stress data (Roden, and Willebrand, private communications), so that one has $S_\tau = -S'_\tau$ and $C = F_\tau(0)$, with $\int dk\ S(k) = 1$. Note that at low latitudes (say, up to 25°N), the wind stress divergence might become nearly comparable to the wind stress curl (Roden, 1974; Düing *et al.*, 1977), which would decrease the magnitude of the oceanic response spectra by a factor of 2. For $S_\tau(k)$, we choose the particular normalized form

$$S_\tau(k) \approx \begin{cases} \frac{3}{4}k_b^{-3}k^2, & 0 \leq k \leq k_b \\ \frac{3}{4}k_b k^{-2}, & k_b \leq k \leq k_c \\ 0, & k > k_c \end{cases} \quad (6.4)$$

with $k_b \ll k_c$. Here $k_b = 2\pi/5000\ \text{km}^{-1}$ is a wavenumber *magnitude* characteristic of baroclinic instability in the atmosphere and k_c some high wavenumber cutoff that need not be specified as long as it is larger than the high wavenumber limit k_m of the oceanic motions considered in this study. The model (6.1) seems plausible and yields zonal wavenumber spectra $F_{\tau_\alpha\tau_\alpha}(k_1,\omega)$ that remain approximately constant for $k \ll k_b$, with a weak maximum near $k_1 = 2\pi/6000\ \text{km}^{-1}$, and decay as k^{-2} for $k_b < k < k_c$. A -2 slope appears appropriate for midlatitudes. In principle, these spectra include storm and hurricane effects, since they are based on long-term statistics of the meteorological fields. However, no information on wavenumber spectra at the hurricane scales were available, and our model is based on simple extrapolations. At high latitude, the spectral decay is stronger, hence we shall consider a model with a k^{-3} decay in the range $k_b \leq k \leq k_c$. To avoid confusion, results pertinent to this latter wind stress model will only be given in brackets. We shall also indicate in Section 7 how sensitive the oceanic response is to the particular model chosen for the atmospheric forcing function.

From Table 2, we choose

$$F_\tau(0) = 10^4\ \text{N}^2\ \text{m}^{-4}\ \text{Hz}^{-1} \quad (6.5)$$

as a characteristic white noise level in midlatitudes. This value will be multiplied by a factor of 3 when representing high-latitude conditions.

b. Wind stress curl

In midlatitudes, the wind stress curl spectrum takes the form

$$F_{\text{curl}\tau}(k,\omega) = F_\tau(0)\ k^2\ S_\tau(k). \quad (6.6)$$

This formula allows us to calculate the *available* white noise level of the wind stress curl contributed by scales in a given wavenumber range. For instance, the available white noise level in the quasi-geostrophic eddy range limited by $k_m = 2\pi/4000\ \text{km}^{-1}$ and $k_M = 2\pi/50\ \text{km}^{-1}$ is given by

$$F^{\text{av}}_{\text{curl}\tau}(0) \approx \tfrac{3}{4}k_b k_M F_\tau(0) = 10^{-6}\ \text{N}^2\ \text{m}^{-6}\ \text{Hz}^{-1} \quad [2\times 10^{-7}]. \quad (6.7)$$

Notice the lower white noise level in high latitudes due to the k^{-3} slope, notwithstanding the increased variance of the wind stress. Relation (6.6) is consistent with the wind stress curl data discussed in Section 5, when the observed values of $F_\tau(0)$ are taken, and integration limits appropriate to the geometry are chosen. Taking $2\pi/350\ \text{km}^{-1}$ as highest wavenumber in (6.6), one recovers the white noise level observed by Düing *et al.* (1977). On the other hand, (6.6) gives a white noise level higher by a factor of 3 than observed by Willebrand (1978), if we take $2\pi/1500\ \text{km}^{-1}$ and $2\pi/5000\ \text{km}^{-1}$ as integration limits.

c. Pressure

Since the large-scale winds are quasi-geostrophic, a consistent model of the pressure spectrum is given by

$$S_p(k) \approx \begin{cases} \frac{3}{4}k_b^{-1}, & 0 < k \leq k_b \\ \frac{3}{4}k_b^3 k^{-4}, & k_b \leq k \leq k_c \\ 0, & k > k_c. \end{cases} \quad (6.9)$$

At high latitudes, we consider a model with a k^{-5} decay in the range $k_b \leq k \leq k_c$. From Table 2, we choose

$$F_p(0) = 4\times 10^{11}\ \text{N}^2\ \text{m}^{-4}\ \text{Hz}^{-1} \quad (6.10)$$

as characteristic white noise level in midlatitudes, and $10^{12}\text{N}^2\text{m}^{-4}\text{Hz}^{-1}$ in high latitudes.

d. Atmospheric forcing function

From (2.38) we can now compute the ratio $\delta(k,\omega)$ of the pressure and wind stress contributions to the power spectrum of the atmospheric forcing function:

$$\delta = \frac{\rho_0^{-2} f_0^{-2} \omega^2 F_p(k,\omega)}{\rho_0^{-2} f_0^{-4} g^2 F_{curl\tau}(k,\omega)} = A\left(\frac{\omega}{f_0}\right)^2 \left(\frac{k_b}{k}\right)^4, \quad (6.10)$$

with

$$A = f_0^4 g^{-2} k_b^{-2} F_p(0)/F_\tau(0) = 6,$$

$$[A = \tfrac{2}{3} f_0^4 g^{-2} k_b^{-2} F_p(0)/F_\tau(0) = 15] .$$

In the quasi-geostrophic eddy wavenumber-frequency range, one has $k > k_b$, $\omega \ll f_0$, so that wind stress forcing strongly dominates the atmospheric forcing function. Pressure forcing is most efficient at very low wavenumbers and high frequencies, yet it can always be neglected in the $\mathbf{k},\omega$ range considered here. Indeed, at $k = k_m$, the value $\delta = 1$ is only reached for periods of the order of 1 day, shorter than those considered here. The inefficiency of the pressure forcing has been suggested by McWilliams (1974) and Magaard (1977). In the following, we neglect F_p and use as power spectrum of the atmospheric forcing function in midlatitudes

$$F(k,\omega) = \rho_0^{-2} g^2 f_0^{-4} k^2 S_\tau(k) F_\tau(0), \quad (6.11)$$

with $S_\tau(k)$ and $F_\tau(0)$ given by (6.3) and (6.4). This spectrum is white in both wavenumber and frequency space, in the ranges of interest here. In high latitudes the spectrum is slightly red ($\sim k^{-1}$) in wavenumber space.

7. Oceanic response

The energy transfer rates by stochastic resonant forcing and the off-resonance response spectra can now be estimated by introducing (6.11) into the formulas derived in Section 4.

a. Barotropic response

Barotropic Rossby waves of 4000 km wavelength can have periods as short as 6 days. Thus, one has $\omega \lesssim \omega_0^{\max}$ in the wavenumber-frequency range considered here, and the barotropic response is resonant. The integrated energy transfer rate (4.13) in midlatitudes (high latitudes) is

$$\frac{\partial}{\partial t} E^0_{\text{tot}} = \tfrac{1}{2}\rho_0^{-1} h^{-1} F_\tau(0) \int_{\pi/2}^{3\pi/2} d\theta \times \int_{k_m}^{k_M} dk \frac{k^2}{k^2 + R_0^{-2}} S_\tau(k)$$

$$\approx \frac{3\pi}{8} \rho_0^{-1} h^{-1} k_b k_m^{-1} F_\tau(0)$$

$$= 3 \times 10^{-4} \text{ W m}^{-2} \quad [6 \times 10^{-4}] \quad (7.1)$$

if $h = 5 \times 10^3$m. For $k \gg R_0^{-1}$, most of the barotropic energy is kinetic [cf. (4.6)] and (7.1) shows that stochastic forcing by the atmosphere yields an increase of the barotropic velocity variance at each level of 1 cm^{2}s^{-2} in 10 days (5 days).

The result (7.1) is independent of the stratification and inversely proportional to the ocean depth. No latitudinal variations are expected other than those due to the variations in the wind stress model, since f_0 does not enter relation (7.1). The integrated energy transfer rate is fairly insensitive to the choice of the spectral slopes of the wind stress model. Using a k^{-3} slope instead of a k^{-2} slope at $k > k_b$ decreases (7.1) by 35% only; assuming white behavior at $k < k_b$ (instead of k^2) also decreases (7.1) by 35%.

The wavenumber dependence of the barotropic response is the same as the one of the wind stress, i.e., proportional to $k^{-2}[k^{-3}]$. Hence, the energy is mainly transferred to long Rossby waves by resonant forcing. In mid-latitudes, 50% of the input is in wavelengths >2000 km, 75% in wavelengths >1000 km. In high latitudes, 75% of the input is in wavelengths >2000 km, 94% in wavelengths >1000 km. Large-scale Rossby waves have the highest frequencies, where our assumption of whiteness and symmetry of the forcing spectrum is least valid. This could lead to an overestimation of the energy transfer rate (7.1) by a factor of 2 or 3 in high latitudes.

b. Baroclinic response

For $\omega \leqslant \omega_1^{\max}$ [$\approx 2\pi/156$ day^{-1} in the MODE region], the baroclinic response is resonant. The integrated energy transfer rate (4.15) is

$$\frac{\partial}{\partial t} E^{bc}_{\text{tot}} = \tfrac{1}{2}\rho_0^{-1} h^{-1} F_\tau(0) \int_{\pi/2}^{3\pi/2} d\theta \times \int_{k_m}^{k_M} dk (\pi R_1 k \coth \pi R_1 k - 1) S_\tau(k)$$

$$= \frac{3\pi}{8} \rho_0^{-1} N_0 f_0^{-1} k_b F_\tau(0) \int_{y_m}^{y_M} dy \times (y^{-1} \coth y - y^{-2})$$

$$= 1.5 \times 10^{-4} \text{ W m}^{-2} \quad [10^{-5}], \quad (7.2)$$

with $y = \pi R_1 k$. For midlatitudes, we have taken $f_0 = 7\ 10^{-5}$ s^{-1} and $N_0 = 2\ 10^{-3}$ s^{-1} as characteristic values. The integral was estimated numerically; its value is 2.3. This integral increases approximately as the logarithm of the high wavenumber cutoff k_M but depends very little on k_m. For high latitudes, we took $f_0 = 10^{-4}$ s^{-1} and the weaker stratification $N_0 = 10^{-3}$ s^{-1}. Since the input rate (7.2) increases with N_0 and decreases with f_0, both effects tend to decrease the baroclinic response in high latitudes. The integrated baroclinic energy transfer rate is sensitive to the choice of the high-wavenumber slope of the wind stress model; using a k^{-3} slope instead of k^{-2} reduces the input rate by a factor of 8. The dependence on the low-wavenumber part of the wind stress model is weak, as in the barotropic case. Finally, it was remarked in Section 3 that by using

a constant buoyancy frequency ocean, we neglect the near-surface amplification of the response for realistic stratification. In the MODE region, the underestimation of (7.2) is by a factor of 4. Thus energy is transferred resonantly into barotropic and baroclinic modes at comparable rates in midlatitudes. In high latitudes, the barotropic energy transfer rate is larger than the baroclinic one.

The wavenumber dependence of the baroclinic response is determined by the product of the transfer function (4.16) and the forcing spectrum (6.11). For $k < R_1^{-1}$, the baroclinic response is proportional to k^0 [k^{-1}], whereas at high wavenumbers ($k \gg \pi R_1^{-1}$) it is proportional to k^{-1} [k^{-2}]. In midlatitudes, most of the energy is transferred to scales comparable to or smaller than the Rossby radius of deformation R_1 ($k \geq R_1^{-1}$). It can be shown that 38% of the integrated energy transfer rate goes into the first baroclinic mode and 17% into the second one. In high latitudes, most of the energy is transferred to intermediate and large scales (in the range $k_m \leq k < R_1^{-1}$); 58% of the energy input goes into the first baroclinic mode, 16% in the second.

For frequencies larger than $\omega_1^{\max}$, the baroclinic response is off-resonant. If all dynamical processes neglected here were of secondary importance, the total energy spectrum for $\omega \gg \omega_1^{\max}$ would be given by

$$E_{\text{tot}}^{bc}(\omega) = \tfrac{1}{2}\rho_0^{-1}h^{-1}[F_\tau(0)/\omega^2] \times \int_{k_m}^{k_M} dk(\pi R_1 k \coth \pi R_1 k - 1)S_\tau(k)$$

$$= 4 \times 10^{-4}\omega^{-2}\,\text{W m}^{-2}\,\text{s}^{-1}\,\text{Hz}^{-1}\ [2 \times 10^{-5}\omega^{-2}].$$

Again, a spectral decay in ω^{-2} is predicted with increasing level at lower latitudes. Other spectra have a similar ω^{-2} behavior, as illustrated in Section 8.

8. Comparison with data

a. Field observations

The spectral characteristics of the quasi-geostrophic eddy field are best documented for the western North Atlantic (e.g., Richman *et al.*, 1977; Schmitz, 1978). In this region, the field is strongly nonhomogeneous and the eddy energy is observed to increase rapidly approaching the Gulf Stream. Because the ocean western boundary is also nearby, it is difficult to assess the relative importance of stochastic atmospheric forcing in generating the eddies without considering their complete energy balance, thereby including nonlinear interactions and topographic influences (known to induce fast exchanges of energy among different scales and modes), propagation effects (causing a westward intensification of the eddy field), energy sources and sinks. This is out of reach at present.

Nevertheless, a crude estimation of the importance of *local* atmospheric forcing can be attempted by comparing the predicted total energy transfer rates (7.1) and (7.2) to the observed eddy energy. Estimates of the eddy kinetic energy (KE) at different sites and depths are given by Schmitz (1978). If we assume for simplicity that the KE at 4000 m depth is representative of the barotropic eddy energy, we find that the total barotropic eddy energy varies from less than 5×10^2 J m^{-2} near 28°N, 65–55°W (the least energetic sites for which data are presently available in the western North Atlantic) to 5×10^3 J m^{-2} near 28°N, 70°W (the MODE region) and higher values closer to the Gulf Stream. Dividing these energies by the transfer rate (7.1), we obtain a characteristic time τ^0 that measures the efficiency of local stochastic forcing by the atmosphere. At the least energetic site τ^0 is rather short (38 days); hence local forcing by the wind might be a dominant generating mechanism for barotropic eddies. In the MODE and more energetic regions, τ_0 is at least 10 times larger and local atmospheric forcing seems negligible for barotropic motions. A similar analysis is more speculative for baroclinic motions, because the available potential energy (APE) is difficult to evaluate. Schmitz gives crude estimates of the vertically integrated kinetic energy in the MODE region (10^4 J m^{-2}) and near 28°N, 55°W (2.5 10^3 J m^{-2}). Here we assume for simplicity that these are estimates of the baroclinic KE. From extensive density surveys during MODE, Fofonoff (private communication) has estimated[3] APE = 2.4 10^4 J m^{-2}, yielding 3.4 10^4 J m^{-2} for the total baroclinic energy. If we divide by (7.2), we find a characteristic time τ^{bc} = 7 years which represents about 17 "minimum wave periods". Thus, *local* stochastic forcing of baroclinic motions does not seem too important in this region. Toward the east, the decay in APE is not as rapid as in deep water KE (Richman *et al.*, 1977). Near 28°N, 55°W, the APE seems, nonetheless, about twice smaller than in the MODE region. Thus, we obtain 1.5 10^4 J m^{-2} as a rough guess for the total baroclinic energy, and τ^{bc} = 3 years. Since the dominant time scale in this region is larger than further west, local stochastic forcing seems important. In the proximity of the Gulf Stream, the observed eddy energy is very large and our estimated input rates give a negligible contribution. Note, however, that it has been suggested recently that the Gulf Stream is an important site of cyclogenesis in the atmosphere, so that the intensity of the atmospheric forcing might be locally enhanced.

Our *tentative* suggestion is therefore that local

[3] The near-surface (first 150 m) contribution to the APE is strongly underestimated in this calculation. This should not matter much here since we want an estimate of the energy of the interior flow. Moreover, the estimate (7.2) also neglects the near-surface amplification of the baroclinic response (cf. sections 3 and 6).

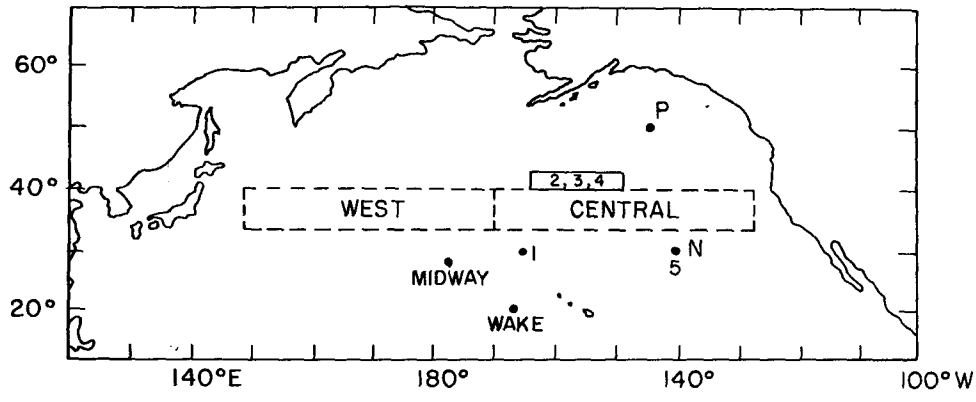

FIG. 9. Location of the North Pacific measurements discussed in this study. The dashed line delineates the regions where the XBT sections in Fig. 12 have been obtained.

stochastic forcing by the wind stress is important for both barotropic and baroclinic motions in the western North Atlantic regions with low eddy activity, but is negligible in regions of high eddy activity. Where to separate these regions cannot be inferred from our analysis.

The central North Pacific is another region of low eddy activity. Since this region is remote from boundaries and from major currents and topographic features, one may expect that the eddy energy is not rapidly redistributed in $\mathbf{k},\omega$ space, and that the observed spectral characteristics of the eddy field can be compared to the predictions of our linear theory. Roden (1977) observed that the amplitude of the disturbances of dynamic height were smaller in the central North Pacific (say, between 170° and 155°W), than in the western part, with a southward increase toward the trade wind region (see North Pacific map on Fig. 9). In the central North Pacific the dominant length scale of the (baroclinic) perturbations was between 400 and 600 km, almost independent of depth, and the perturbation amplitudes were much larger in the sections taken in winter and fall than in the sections taken in the spring. Roden has therefore suggested that these baroclinic fluctuations were due to direct wind stress forcing.

Since the pycnocline is very shallow in the central North Pacific, the radius of deformation for baroclinic modes is small (Roden chooses $R_1 \approx 10^4$m) and baroclinic resonance can only occur in midlatitudes at periods of a few years or more. On smaller time scales the baroclinic response must be forced. The properties of the subsurface temperature or vertical displacement spectra may be inferred from our analysis in Section 3. Assuming that the buoyancy frequency is approximately constant and that the vertical displacement is due to the baroclinic modes only, we find for the vertical displacement

$$\xi(\mathbf{k},x_3,\omega) = -i\frac{f_0 g^{-1} Q(\mathbf{k},\omega)\,\sinh[(x_3+h)k\pi R_1/h]}{\omega\,\sinh k\pi R_1} \quad (8.1)$$

if $\omega \gg \omega_1(\mathbf{k})$. Here we have used (2.14), (2.27) and summed the normal mode decomposition (3.12) over the baroclinic modes only. Note that the solution (8.1) is exponentially decaying as observed by Roden (1977). Near the surface, $x_3 \approx 0$ and $\xi(\mathbf{k},0,\omega) \approx i\,W_E/\omega$, where W_E denotes the Ekman suction velocity (2.36). This latter expression was used by Frankignoul and Hasselmann (1977) to discuss the frequency spectra of subsurface temperature in the central North Pacific, mainly at 150 m depth, as given by Bernstein and White (1974). The observed spectra were consistent with the predicted ω^{-2} behavior, but the relatively high energy level was difficult to explain by stochastic wind forcing. Our new estimate (6.7) of wind stress curl energy density is, however, higher and the discrepancy is reduced to about a factor of 3 (Fig. 10). This is within the uncertainty of our calculations, especially if one takes into account that the data were of short duration and mainly taken in winter, when the atmospheric forcing is most intense.

Bernstein and White (1977) have calculated zonal wavenumber spectra of temperature *anomalies* at 300 m depth from repeated XBT sections along latitude circles in the North Pacific, between 33 and 40°N. The spectrum for the western North Pacific (west of 170°W) is one order of magnitude higher than for the central and eastern parts (between 170° and 140°W) (Fig. 11). In contrast to the spectrum in the western part (thin line) which shows a peak near 1000 km wavelength, the spectrum for the central North Pacific (thick line) is rather flat, decaying only slowly with increasing zonal wavenumber. The smooth line in Fig. 11 shows that the model prediction

$$F_\xi(k_1, x_3 = 0, \omega)\delta(k_1 - k_1')\delta(\omega - \omega') \equiv \int_{-\infty}^{\infty} dk_2 \langle \xi(\mathbf{k}, x_3 = 0, \omega)\xi^*(\mathbf{k}', x_3 = 0, \omega')\rangle$$

is consistent with the observed *spectral slope* in the central North Pacific. The *level* of the predicted spectrum is arbitrary and cannot be estimated with-

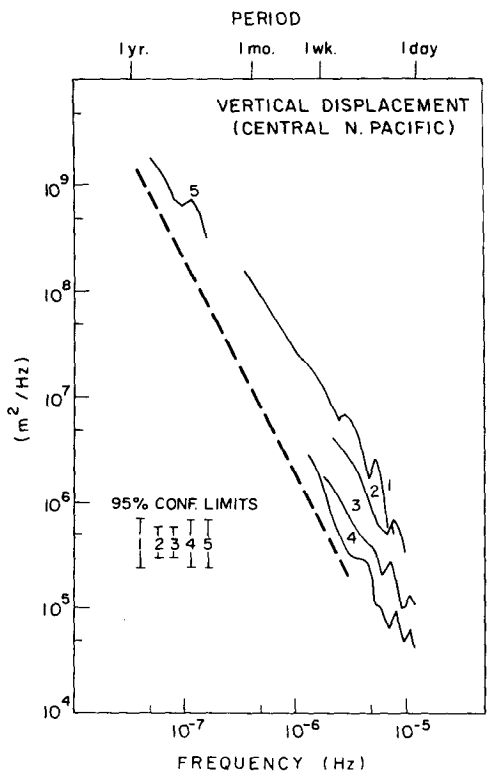

FIG. 10. Spectra of vertical displacement at various stations in the central North Pacific between 30 and 43°N, 165 and 140°W at depths of 150 m (1–4) and 200 m (5) [after Bernstein and White, (1974) cf. Fig. 9]. We have assumed a temperature stratification of 5×10^{-2} °C m^{-2}. Data 1, 2 and 4 were taken in winter, data 3 in summer, and data 5 (OWS N) covers nine years. The dashed line shows the model prediction.

out additional assumptions [the response spectrum is red with respect to frequency, cf. Eq. (4.10)] but the hypothesis of dominant atmospheric forcing can be tested by comparing the *seasonal variability* of the oceanic signal to that of the forcing function. Five XBT sections in the central North Pacific were taken during fall and winter, four during spring and summer. We have constructed from the individual spectra (Bernstein and White, private communication) averaged spectra for these two periods (dashed and dotted lines in Fig. 11). At wavelengths shorter than 1000 km, the winter-fall spectrum is about three times higher than the spring-summer one. This seasonal variability cannot be explained by the slight shift in the mean latitude of the sections (~2°) but strikingly corresponds to the seasonal variability of the white noise level of the wind stress at Weathership P (Fig. 12). Thus, stochastic forcing by the atmosphere seems a dominant generating mechanism for baroclinic eddies in the central North Pacific. Because of inadequate XBT sampling in time, the seasonal variability of the western North Pacific could not be investigated.

The stochastic forcing models predict that atmospheric and oceanic variables will be correlated. In the off-resonance case, the predicted correlations are small, unless smoothed data are used (Frankignoul and Hasselmann, 1977). In the resonant case, smaller correlations are expected if waves propagate away from the forcing region. Some measurements suggest a significant coherence between atmospheric (pressure, wind stress or air temperature) and oceanic (temperature or current at depth) variables at high frequencies (i.e. ~10-day period) which is consistent with the large barotropic response predicted by our model. There is no evidence of correlation at low frequencies, but the data base is inadequate and correlations will be very difficult to detect in the presence of many internal modes. High-frequency coherence is reported by Ivanov and Byshev (1972) for Weathership D (44°N, 41°W) and by Byshev and Ivanov (1974) for the POLYGON data taken in the tropical North Atlantic (16°N, 33°W). Note, however, that these data are very noisy. Wunsch (1972) analyzed sea level fluctuations at Bermuda (32°N, 65°W) and suggested that no oceanic normal modes were excited by pressure fluctuations at periods <12 days. He also found no significant coherence between atmospheric pressure and subsurface temperature in the period range 1–25 months. However, Bermuda, like Weathership D,

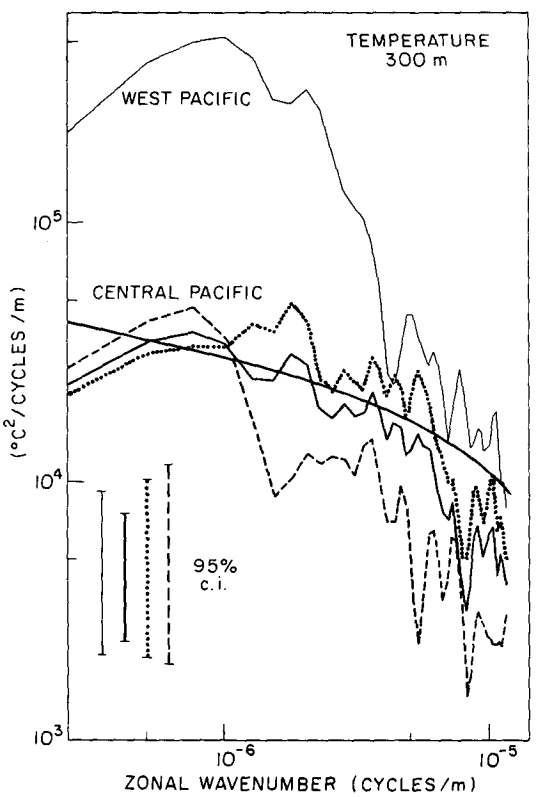

FIG. 11. Zonal wavenumber spectra of temperature at 300 m depth in the North Pacific, computed from zonal XBT sections taken between 35 and 40°N (Fig. 9). Thin line: west of 170°W, thick line: east of 170°W. The dotted line shows the spectrum computed from sections in fall and winter, the dashed line the spectrum computed from sections in spring and summer [after Bernstein and White (1977 and private communication)].

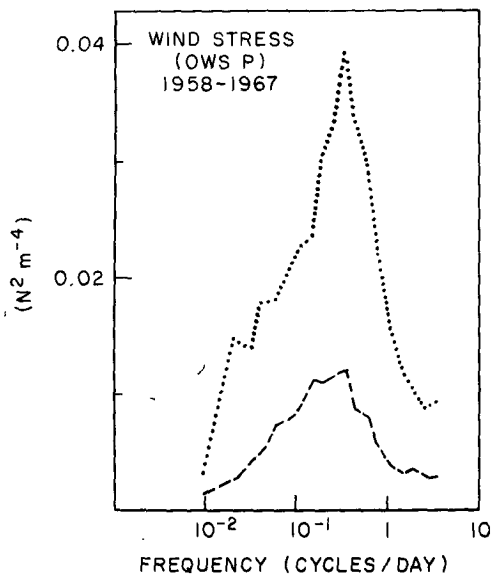

FIG. 12. Variance-conserving plot of the wind stress spectrum at OWS P (see Fig. 5) during spring–summer (dotted line) and fall–winter (dashed line) (after Fissel, 1975).

is in the proximity of the Gulf Stream, and Gulf Stream rings and extension rings may dominate the low-frequency phenomena. In a region further away from the Gulf Stream influence (around the Gillis seamount at 35°N, 59°W), P. I. Taylor (private communication) observed recently the intensification of bottom currents (at 5 km depth) during the passage of hurricanes. The high-frequency coupling between local atmospheric forcing and deep currents seems stronger in high latitudes as expected from (7.1). Meincke (1976) observed a significant coherence between atmospheric pressure and near-bottom currents on the Iceland-Faroe Ridge. Baker *et al.* (1977) (see also Baker, 1977) detected a significant coherence between geostropic wind, wind stress and deep currents in the Drake Passage, and suggested that the scale of the phenomenon was large. It should be remarked that these high-latitude data were both taken in regions with strong topographic features, for which our analysis may not be applicable (see also Philander, 1978).

b. Oceanic models

Faller (1966) has estimated from average wind stress data that the rate of energy input from the *mean* atmospheric circulation into the *mean* oceanic circulation is about 3×10^{-3} W m^{-2}. Using a two-layer ocean model, Gill *et al.* (1974) suggested (analytically) that the energy input rate[4] into the wind-driven Sverdrup flow is $\sim 10^{-3}$ W m^{-2}. The energy budget of several oceanic GCM experiments with idealized basin geometry and atmospheric forcing is discussed by Holland (1975). For baroclinic oceans, most of the (steady) wind energy goes into mean baroclinic motions (from 17 to 24 10^{-4} W m^{-2} in the cases discussed), whereas little energy goes into mean barotropic motions (from 0.4 to 3 10^{-4} W m^{-2}). Recently, Bryan (private communication) made an experiment with a GCM of the world ocean (2° resolution) with realistic coastlines and bottom topography, using Hellerman's (1967) observed data for the wind stress forcing. The computed energy transfer rates of 21×10^{-4} and 26×10^{-4} W m^{-2} for the Northern and Southern Hemispheres, respectively, seems the most reliable estimates of the energy input rate from the mean atmospheric to the mean oceanic circulation. These are only one order of magnitude larger than our estimates of the energy input rate from the stochastic atmospheric fluctuations into quasi-geostrophic eddies.

With the development of eddy resolving models (EGCM), the energy conversion from mean into fluctuating motions has also been explored. Table 3 summarizes some results of EGCM experiments. In all cases the wind forcing is steady, eastward and sinusoidal, but its meridional scale varies (see the number of gyres). The thermal forcing has a fluctuating component, but its effect has not been discussed. Eddy energy is released via baroclinic, barotropic or mixed baroclinic-barotropic instability. Unfortunately, the energetic properties of ocean models are strongly dependent on the model physical assumptions and parameter values (cf. Robinson *et al.*, 1977). In particular, the energy input rate into eddies varies by more than one order of magnitude in the experiments reported in Table 3, and it is difficult to decide which value is representative of oceanic conditions. However, comparison with GCM's, especially the recent results of Bryan (see above), suggests that the experiments with the largest input rates strongly overestimate the energy input into the mean oceanic circulation. Thence, our estimates (7.1) and (7.2) of the energy input into the eddy field by stochastic atmospheric forcing seem smaller, but comparable to the input rate by instability of the general circulation.

9. Summary and conclusions

We have attempted to estimate quantitatively the quasi-geostrophic response of the ocean to stochastic forcing by wind stress and atmospheric pressure, in order to evaluate the importance of this mechanism in generating oceanic eddies. Our analysis has been simplified by a variety of assumptions. We have considered the linear response of a continuously stratified β-plane ocean and neglected the effects of lateral boundaries, bottom topography, mean currents and horizontal inhomogeneities. Be-

[4] The numbers given in this section only include the large-scale circulation below the Ekman layer.

TABLE 3. Energy transfer rates in selected EGCM experiments. Dominant instability refers to the main process of eddy generation, the amplitude of the applied sinusoidal wind stress is given and sG indicates that the wind stress pattern creates s gyres. KE is the kinetic energy, APE the available potential energy.

Model	Domain geometry	Vertical resolution	Forcing τ	Input rates (10^{-4} W m^{-2}) Into mean KE (Into mean APE)	Into eddies KE + APE	Dominant instability	Comments
Holland and Lin (1975)	1000 × 1000 km flat bottom	2 layers	(0.1 Nm^{-2}, 1G)	14 (−)	3	baroclinic	Experiment 1
Han (1975)	4000 × 4000 km flat bottom	5 levels	(0.2 Nm^{-2}, $1^{1/2}G$)	71 (69)	34	mixed	
Robinson *et al.* (1977)	2000 × 2000 km flat bottom	5 levels	(0.4 Nm^{-2}, 1G)	213 (not given)	8* (*KE only)	barotropic	APE not given
Semtner and Mintz (1977)	3000 × 2000 km flat and continental shelf	5 levels	(0.3 Nm^{-2}, $2^{1/2}G$)	~16.4 (~70)	~57	mixed	
Holland (1978)	1000 × 2000 km flat bottom (quasi-geostrophic)	2 layers	(0.1 Nm^{-2}, 2G)	16.4 (−)	10	barotropic	Experiment 3
			(0.1 Nm^{-2}, 2G)	18.3 (−)	16.5	barotropic	Experiment 5
			(0.4 Nm^{-2}, 2G)	221 (−)	181	barotropic	Experiment 8

cause of the linearity of the model, the oceanic response spectra are completely determined by the spectra of the atmospheric fields. Thus, the observed structure of the atmospheric variables in the wavenumber-frequency range of quasi-geostrophic oceanic motions has been thoroughly reviewed. Because of the short correlation time scale of the atmospheric variables, the spectrum of the atmospheric forcing fields is to a reasonable approximation white in frequency space and symmetric. For simplicity, we have assumed homogeneity of the forcing fields. Latitudinal variations were nonetheless represented in a crude fashion, by using larger variance and steeper high wavenumber fall-off in high latitudes (e.g., wind stress decaying like k^{-2} and k^{-3} in mid and high latitudes, respectively). The wind stress was found to be the dominant forcing mechanism (Ekman pumping).

The oceanic response has been estimated using expansion of the oceanic streamfunction into vertical normal modes. Because of the (quasi) symmetry of the wind stress in the wavenumber-frequency range of quasigeostrophic oceanic eddies, westward propagating Rossby waves can be resonantly excited. The barotropic response is resonant at practically all frequencies. The baroclinic response is resonant at low frequencies ($\omega < 2\pi/150$ day^{-1} in the North Atlantic). At moderate and high frequencies, the baroclinic response to stochastic forcing is off-resonant. The baroclinic frequency spectra then behave as ω^{-2}. To circumvent the specification of dissipation and transfer mechanisms in the ocean interior, we have calculated energy transfer rates in the resonant case. The dependence on the oceanic stratification and on the model spectrum of the atmospheric forcing fields was reduced by considering the depth-integrated response of the ocean, by integrating this response over horizontal wavenumber (in the range $2\pi/4000$ km$^{-1} \leq k \leq 2\pi/50$ km^{-1}) and by summing the contributions of all baroclinic modes.

In midlatitudes, we find that the total energy transfer rate by stochastic forcing of barotropic motions is of the order of 3×10^{-4} W m^{-2}. Most of the energy is transferred into long barotropic Rossby waves. The resonant energy transfer rate into baroclinic motions is comparable, and half of this energy goes into the first two baroclinic modes. In high latitudes, the energy input rate into barotropic modes remains of the order of 3×10^{-4} W m^{-2}, but the input rate into baroclinic motions is smaller (at least 10^{-5} W m^{-2}), and most of this energy is transferred to the first two baroclinic modes. The barotropic response is not too dependent on our many simplifying assumptions, but the baroclinic response depends fairly sensitively on the wavenumber spectrum of the atmospheric fields.

The total input rate by stochastic atmospheric forcing is only an order of magnitude smaller than the energy input from the mean atmospheric fields into the oceanic general circulation, and it appears to be smaller, but comparable with the rate of energy conversion from the mean circulation into quasi-geostrophic eddies, by barotropic and baroclinic

instabilities. Since these instabilities mainly occur in the vicinity of the intense boundary currents, we expect that stochastic forcing by the wind is a dominant generating mechanism for the eddies only in the central part of the oceans. Observations of subsurface temperature fluctuations in the central North Pacific (frequency spectra, wavenumber spectra and their seasonal variations) and data in the western North Atlantic are consistent with this suggestion. Therefore, stochastic forcing by the atmosphere should be included in studies of mid-ocean dynamics. This may be particularly important in EGCM models, since they are generally tuned to produce a "realistic" eddy field without the random forcing.

Our approach has obvious deficiencies: lateral boundaries should be included, especially for calculating the barotropic response since barotropic waves travel so fast that they feel the boundaries. There may also exist a considerable response at larger scales than considered here, for example of cutoff waves (Longuet-Higgins, 1965). However, these waves are not adequately modeled by the β-plane approximation, and the spherical geometry of the earth should be considered. Also, the anisotropy and inhomogeneity of the forcing should then be introduced. This is why we have not discussed possible implications for climatic changes. The forcing spectra are white (and eventually become red) down to the lowest frequencies, so that long, low-frequency baroclinic waves might induce significant climatic fluctuations.

The choice of a flat-bottomed ocean also introduces some limitations to the applicability of our results, because bottom topography strongly affects the kinematics and dynamics of quasi-geostrophic eddies (e.g., McWilliams, 1974; Rhines, 1977; Philander, 1978). As noted by Philander, the topography will alter the oceanic response spectra by scattering the large-scale motions into smaller eddies and by supporting a new class of waves. However, it should be stressed that the former effect will change the wavenumber structure of the response but not the integrated energy input rates. Our goal was to estimate how much energy is transferred into the deep ocean by stochastic atmospheric forcing. How this energy is redistributed by other processes depends on the wavenumber structure of the response, but this question is beyond the scope of the present paper.

Acknowledgments. We would like to thank Prof. K. Hasselmann for useful suggestions and discussions, Prof. S. K. Kao for generously computing some of the atmospheric spectra presented in this study, and Prof. J. Charney for his help. Data, some of them unpublished, and (or) comments were kindly provided by Drs. R. Bernstein, G. Flierl, N. Fofonoff, D. Luther, E. Mehr, R. Pratt, W. White, J. Willebrand, C. Wunsch and others who are gratefully acknowledged. This research was undertaken when one of us (C.F.) was at the Max Planck Institut für Meteorologie, Hamburg. This author was later supported by the National Science Foundation, Office of IDOE, under Grants OCE 74-19782 and OCE 77-28349. This is a contribution of the Sonderforschungsbereich 94, Meeresforschung Hamburg, and MODE No. 98.

REFERENCES

Andrews, D. G., and B. J. Hoskins, 1978: Energy spectra predicted by semi-geostrophic theories of frontogenesis. *J. Atmos. Sci.*, **35**, 414–432.

Baker, D. J. Jr., 1977: High latitude processes for ocean climate modeling. *Proc. JOC/SCOR Conf. on General Circulation Models of the Ocean and Their Relation to Climate*, Helsinki, WMO, Vol. 1, 306–337.

——, W. D. Nowlin, Jr., R. D. Pillsbury and H. L. Bryden, 1977: Antarctic circumpolar current: Space and time fluctuations in the Drake passage. *Nature*, **268**, 696–699.

Bernstein, R. L., and W. B. White, 1974: Time and length scales of baroclinic eddies in the central North Pacific ocean. *J. Phys. Oceanogr.*, **4**, 613–624.

—— and ——, 1977: Zonal variability of the distribution of eddy energy in the mid-latitude North Pacific ocean. *J. Phys. Oceanogr.*, **7**, 123–126.

Blackmon, M. L., 1976: A climatological spectra study of the 500 mb geopotential height of the Northern Hemisphere. *J. Atmos. Sci.*, **33**, 1607–1623.

Brooks, D. A., and C. N. K. Mooers, 1977: Fluctuations in the Florida Current, summer 1970. *Deep-Sea Res.*, **24**, 399–426.

Byshev, V. I., and Yu. A. Ivanov, 1969: The time spectra of some characteristics of the atmosphere above the ocean. *Izv. Akad. Nauk SSR*, **5**, 17–28.

——, and ——, 1974: Some results of the investigation of response of the field of currents to disturbances of the atmosphere. *Atlantic and Hydrophysical POLYGON 70*, Nauka, Moscow, 421 pp.

Charney, J. C., 1971. Geostrophic turbulence. *J. Atmos. Sci.*, **28**, 1087–1095.

Desbois, M., 1975. Large-scale kinetic energy spectra from Eulerian analysis of EOLE wind data. *J. Atmos. Sci.*, **32**, 1838–1847.

Dorman, C. E., 1974. Analysis of meteorological and oceanographic data from Ocean Station Vessel N (30°N, 140°W). Ph D. thesis, Oregon State University, 136 pp.

Düing, W. O., C. N. K. Mooers and T. N. Lee, 1977. Low-frequency variability in the Florida current and relations to atmospheric forcing from 1972 to 1974. *J. Mar. Res.*, **35**, 129–161.

Elsberry, R. L., T. S. Fraim and R. N. Trapnell, Jr., 1976: A mixed layer model of the oceanic thermal response to hurricanes. *J. Geophys. Res.*, **81**, 1153–1162.

Faller, A. J., 1966: Sources of energy for the ocean circulation and a theory of the mixed layer. *Proc. 5th U. S. National Congress Applied Mechanics*, 651–672.

Eissel, D. B., 1975: A frequency analysis of ten years of surface atmospheric data at ocean weathership "Papa" (50°N, 145°W). M.S. thesis, University of British Columbia, 136 pp.

——, S. Pond and M. Miyake, 1976: Spectra of surface atmospheric quantities at ocean weathership P. *Atmosphère*, **14**, 77–97.

Flierl, G. R., 1978: Models of vertical structure and the calibration of two layer models. *Dyn. Atmos. Oceans*, **2**, 341–381.

Frankignoul, C., and K. Hasselmann, 1977: Stochastic climate models, Part II. Application to sea-surface temperature anomalies and thermocline variability. *Tellus*, **29**, 289–305.

Frost, M. R., 1975: Stress, evaporative heat flux and sensible heat flux distributions of the North Atlantic (mid-latitude) and their contribution to the production of large scale sea-surface temperature anomalies. Master's thesis, Southampton University.

Gates, W. L., 1968: A numerical study of transient Rossby waves in a wind-driven homogeneous ocean. *J. Atmos. Sci.*, **25**, 3–22.

Gill, A. E., J. S. A. Green and A. J. Simmons, 1974: Energy partition in the large-scale ocean circulation and the production of mid-ocean eddies. *Deep-Sea Res.*, **21**, 499–528.

Han, Y. J., 1975: Numerical simulation of mesoscale ocean eddies. Ph.D. thesis, UCLA, 154 pp.

Hasselmann, K., 1967: Non-linear interactions treated by the methods of theoretical physics (with application to the generation of waves by wind). *Proc. Roy. Soc. London*, **A 229**, 77–100.

——, 1970: Wave-driven inertial oscillations. *Geophys. Fluid Dyn.*, **1**, 463–502.

——, 1976: Stochastic climate models, Part I, Theory. *Tellus*, **28**, 473–485.

Hellerman, S., 1967: An updated estimate of the wind stress on the world ocean. *Mon. Wea. Rev.*, **95**, 607–626.

Holland, W. R., 1975. Energetics of baroclinic oceans. *Proc. Symp. Numerical Models of Ocean Circulation*, Durham, N. H., Nat. Acad. Sci., Washington, D. C.

——, and L. B. Lin, 1975. On the generation of mesoscale eddies and their contribution to the oceanic general circulation. *J. Phys. Oceanogr.*, **5**, 642–669.

——, 1978: The role of mesoscale eddies in the general circulation of the ocean. Numerical experiments using a wind-driven quasi-geostrophic model. *J. Phys. Oceanogr.*, **8**, 363–392.

Ivanov, Yu. A., and V. I. Byshev, 1972: Statistical analysis of the response of the ocean's temperature field to atmospheric disturbances. *Izv. Akad. Nauk SSR*, **8**, 344–348.

Julian, P. R., and A. K. Cline, 1974. The direct estimation of spatial wavenumber spectra of atmospheric variables. *J. Atmos. Sci.*, **31**, 1526–1539.

Kao, S. K., R. L. Jenne and J. F. Sagendorf, 1970: The kinetic energy of large-scale atmospheric motion in wave-number-frequency space: II. Mid-troposphere of the Southern Hemisphere. *J. Atmos. Sci.*, **27**, 1008–1020.

Kraichnan, R. H., 1967: Inertial ranges in two-dimensional turbulence. *J. Phys. Fluids*, **10**, 1417–1423.

Leetmaa, A., 1978: Fluctuating winds, an energy source for mesoscale motions. *J. Geophys. Res.*, **83**, 427–430.

Longuet-Higgins, M. S., 1965: Planetary waves on a rotating sphere. *Proc. Roy. Soc. London*, **A284**, 40–68.

Magaard, L., 1973: On the generation of internal gravity waves by a fluctuating buoyancy flux at the sea surface. *Geophys. Fluid Dyn.*, **5**, 101–111.

——, 1977: On the generation of baroclinic Rossby Waves in the ocean by meteorological forces. *J. Phys. Oceanogr.*, **7**, 359–364.

Meincke, J., 1976: Coupling between bottom currents and weather patterns on the Iceland-Faroe Ridge. ICES, CM 1976/C:30, Hydrographic Committee.

McWilliams, J. C. 1974: Forced transient flow and small scale topography. *Geophys. Fluid Dyn.*, **6**, 49–79.

MODE Group, 1978: The Mid-Ocean Dynamics Experiments. *Deep-Sea Res.* (in press).

Munk, W. H., and N. Philips, 1968: Coherence and band-structure of interial motion in the sea. *Rev. Geophys.*, **6**, 447–472.

Philander, S. G. H., 1978: Forced oceanic waves. *Rev. Geophys. Space Phys.* **16**, 15–46.

Phillips, N., 1966: Large-scale eddy motion in the Western Atlantic. *J. Geophys. Res.*, **71**, 3883–3891.

Pratt, R. W., 1975: Space-time spectral analysis of large scale mid-latitude disturbances. Ph.D. thesis, University of Washington.

——, 1976: The interpretation of space-time quantities. *J. Atmos. Sci.*, **33**, 1060–1066.

——, and J. M. Wallace, 1976: Zonal propagation characteristics of large-scale fluctuations in the mid-latitude troposphere. *J. Atmos. Sci.*, **33**, 1184–1194.

Rhines, P. B., 1977: The dynamics of unsteady currents. *The Sea*, Vol. 6, E. D. Goldberg, Ed., Wiley, 189–318.

Richman, J. G., C. Wunsch and N. G. Hogg, 1977: Space and time scales of mesoscale motion in the Western North Atlantic. *Rev. Geophys. Space Phys.*, **15**, 385–420.

Robinson, A. R., D. E. Harrison, Y. Mintz and A. J. Semtner, 1977: Eddies and the general circulation of an idealized oceanic gyre: A wind and thermally driven primitive equation numerical experiment. *J. Phys. Oceanogr.*, **7**, 182–207.

——, D. B. Haidvogel and D. E. Harrison, 1979. Mesoscale eddies and general oceanic circulation models. *Dyn. Atmos. Oceans* (in press).

Roden, G. I., 1974: Thermohaline structure, fronts, and sea-air energy exchange of the trade wind region east of Hawaii. *J. Phys. Oceanogr.*, **4**, 168–182.

——, 1977: On long-wave disturbances of dynamic height in the North Pacific. *J. Phys. Oceanogr.*, **7**, 41–49.

Saunders, P. M., 1976. On the uncertainty of wind stress curl calculations. *J. Mar. Res.*, **34**, 155–160.

——, 1977: Wind stress on the ocean over the eastern continental shelf of North America. *J. Phys. Oceanogr.*, **7**, 555–566.

Schmitz, W. J. Jr., 1978: Observations of the vertical distribution of low frequency kinetic energy in the western North Atlantic. *J. Mar. Res.*, **36**, 295–310.

Semtner, A. J., and G. Mintz, 1977: Numerical simulation of the Gulf Stream and mid-ocean eddies. *J. Phys. Oceanogr.*, **7**, 208–230.

Veronis, G., 1970: Effect of fluctuating winds on ocean circulation. *Deep-Sea Res.*, **17**, 421–424.

——, and H. Stommel, 1956: The action of variable wind stresses on a stratified ocean. *J. Mar. Res.*, **15**, 43–75.

Welch, C. S., 1972: On the calculation of wind stress curl over open ocean areas from synoptic meteorological data with application of time dependent ocean circulation. *WHOI* Ref. 72–6, 189 pp.

Willebrand, J., 1978: Temporal and spatial scales of the wind field over North Pacific and North Atlantic *J. Phys. Oceanogr.*, **8**, 1080–1094.

Willson, M. A. G., 1975: A wavenumber-frequency analysis of large-scale tropospheric motions in the extratropical northern hemisphere. *J. Atmos. Sci.*, **32**, 478–488.

Wunsch, C., 1972: Bermuda sea level in relation to tides, weather and baroclinic fluctuations. *Rev. Geophys. Space Phys.*, **10**, 1–49.